Received: 7 December 2023 | Revised: 10 April 2024 | Accepted: 14 April 2024

DOI: 10.1111/ejn.16375

RESEARCH REPORT

EJN European Journal of Neuroscience FENS WILEY

# The olfactory network of larval *Xenopus laevis* regenerates accurately after olfactory nerve transection

**Sara J. Hawkins**[1,2] | **Yvonne Gärtner**[1,2,3] | **Thomas Offner**[1] | **Lukas Weiss**[1] | **Guido Maiello**[4,5] | **Thomas Hassenklöver**[1] | **Ivan Manzini**[1]

[1]Institute of Animal Physiology, Department of Animal Physiology and Molecular Biomedicine, Justus Liebig University Gießen, Gießen, Germany

[2]School of Biological Sciences, Faculty of Environmental and Life Sciences, University of Southampton, Southampton, UK

[3]Department of Neurology, Focus Program Translational Neuroscience (FTN) and Immunotherapy (FZI), Rhine-Main Neuroscience Network (rmn2), University Medical Center of the Johannes Gutenberg University Mainz, Mainz, Germany

[4]Department of Experimental Psychology, Justus Liebig University Gießen, Gießen, Germany

[5]School of Psychology, Faculty of Environmental and Life Sciences, University of Southampton, Southampton, UK

**Correspondence**
Ivan Manzini, Institute of Animal Physiology, Department of Animal Physiology and Molecular Biomedicine, Justus Liebig University Gießen, 35392 Gießen, Germany.
Email: ivan.manzini@physzool.bio.uni-giessen.de

**Present addresses**
Thomas Offner, Zebrafish Neurobiology, European Neuroscience Institute, Göttingen, Germany; and Lukas Weiss, Department of Ecology and Evolutionary Biology, Princeton University, Princeton, New Jersey, USA.

**Funding information**
DFG, Grant/Award Number: 4113/4-1

Edited by: Paola Bovolenta

## Abstract

Across vertebrate species, the olfactory epithelium (OE) exhibits the uncommon feature of lifelong neuronal turnover. Epithelial stem cells give rise to new neurons that can adequately replace dying olfactory receptor neurons (ORNs) during developmental and adult phases and after lesions. To relay olfactory information from the environment to the brain, the axons of the renewed ORNs must reconnect with the olfactory bulb (OB). In *Xenopus laevis* larvae, we have previously shown that this process occurs between 3 and 7 weeks after olfactory nerve (ON) transection. In the present study, we show that after 7 weeks of recovery from ON transection, two functionally and spatially distinct glomerular clusters are reformed in the OB, akin to those found in non-transected larvae. We also show that the same odourant response tuning profiles observed in the OB of non-transected larvae are again present after 7 weeks of recovery. Next, we show that characteristic odour-guided behaviour disappears after ON transection but recovers after 7–9 weeks of recovery. Together, our findings demonstrate that the olfactory system of larval *X. laevis* regenerates with high accuracy after ON transection, leading to the recovery of odour-guided behaviour.

**Abbreviations:** AUC, area under the curve; cAMP, cyclic adenosine monophosphate; MTCs, mitral cells and tufted cells; OB, olfactory bulb; OE, olfactory epithelium; ON, olfactory nerve; ORI, odourant response index; ORNs, olfactory receptor neurons; OS, olfactory system.

**KEYWORDS**
glomerular clusters, odourant responses, olfactory behaviour, olfactory receptor neurons, reinnervation

## 1 | INTRODUCTION

Across vertebrate species, neurogenesis occurs well beyond embryonic stages but only in some regions of the nervous system (Breer, 2003; Buck & Axel, 1991; Gaillard et al., 2004; Manzini et al., 2022; Spehr & Munger, 2009). The olfactory system (OS) is one region that shows neurogenesis throughout life (Brann & Firestein, 2014), making it an ideal model system for studying neuronal network formation, function and regeneration (Manzini, 2015; Manzini et al., 2022; Murray & Calof, 1999).

Olfaction is a form of chemosensation in which molecules in the environment directly interact with olfactory receptors expressed by olfactory receptor neurons (ORNs; Breer, 2003; Buck & Axel, 1991; Gaillard et al., 2004; Manzini et al., 2022; Spehr & Munger, 2009). The cell bodies of ORNs are located inside the nasal cavity in the olfactory epithelium (OE). Olfactory receptor neurons extend their axons via the olfactory nerve (ON) into the olfactory bulb (OB) in the anterior telencephalon. When ORNs are activated by the binding of odourants to odourant receptors, synaptic activity occurs in the OB (Buck, 1996; Manzini et al., 2022). Axons of ORNs synapse with bulbar second-order neurons, that is, mitral cells and tufted cells (MTCs), and bulbar interneurons within neuropil clusters called glomeruli (Manzini et al., 2022; Mombaerts et al., 1996; Ressler et al., 1994). Upon activation by ORNs and after various intrabulbar processing steps, MTCs relay olfactory information to higher olfactory centres (Manzini et al., 2022). This sequence of cell activation and processing of olfactory information ultimately gives meaning to the olfactory surroundings and influences behavioural outcomes. Olfactory-guided behaviour is essential for survival and reproduction, specifically in finding mates, shelter and food sources and avoiding predators (Ache & Young, 2005; Dikecligil & Gottfried, 2024; Manzini et al., 2022).

The peripheral location of ORNs permits odourant detection but leaves these neurons vulnerable to potential noxious substances in the surrounding environment. It is assumed that for this reason, these neurons have a limited lifespan (Cowan & Roskams, 2002; Leung et al., 2007) and need to be constantly replaced throughout the life of an animal (Brann & Firestein, 2014; Cowan & Roskams, 2002). To counteract this loss, a pool of stem cells residing in the basal layer of the OE provides new neurons to replenish those lost (Graziadei, 1973; Graziadei & Metcalf, 1971; Schwob et al., 2017). After stem cell proliferation and differentiation, newly formed ORNs must integrate into the OS to maintain olfactory function. Cell death and stem cell proliferation occur both during the process of natural cell turnover (Brann & Firestein, 2014; Graziadei, 1973; Graziadei & Metcalf, 1971) as well as after lesions of the OS (Brann & Firestein, 2014; Schwob, 2002; Schwob et al., 2017). Substantial recovery from lesion to the olfactory circuit has been shown to occur in multiple vertebrate animal models [e.g., mouse (Blanco-Hernández et al., 2012; Cheung et al., 2014; Kobayashi & Costanzo, 2009; McMillan Carr et al., 2004; Schwob, 2002; Schwob et al., 1999; St John & Key, 2003), rat (Graziadei & Monti Graziadei, 1980), hamster (Koster & Costanzo, 1996; Yee & Costanzo, 1995), rabbit (Mulvaney & Heist, 1971), pigeon (Jennings et al., 1995; Oley et al., 1975), salamander (Simmons et al., 1981; Simmons & Getchell, 1981a, 1981b), frog (Graziadei & DeHan, 1973); larval clawed frog (Frontera et al., 2016; Hawkins et al., 2017; Terni et al., 2017) and zebrafish (Calvo-Ochoa et al., 2021; Calvo-Ochoa & Byrd-Jacobs, 2019; Godoy et al., 2020)]. Similar to other vertebrates, in the human OE, a lifelong turnover of ORNs takes place (Brann & Firestein, 2014; Hahn et al., 2005). A certain degree of recovery also occurs in humans after lesions in the OE and ON, however, the recovery is not as efficient as in other vertebrates, especially after ON injuries (Howell et al., 2018; Jiang & Lu, 2019; Reiter et al., 2004).

The general organisation of the *Xenopus* OS is similar to that of other vertebrates (Eisthen, 2002; Manzini et al., 2022; Manzini & Schild, 2010). Nevertheless, some crucial anatomical and functional differences exist between the OSs of *Xenopus* (and amphibians in general) and other vertebrate species (Manzini & Schild, 2010; Weiss, Manzini, et al., 2021; Offner et al., 2023). The molecular and cellular properties of the neural stem cells of the OE and the basic principles controlling cell turnover in the OS are also largely conserved in vertebrates (Hahn et al., 2005; Schwob et al., 2017; Sokpor et al., 2018). As in most other vertebrates, the *Xenopus* OS includes a variety of ORN subtypes that differ in morphology, olfactory receptor expression and transduction mechanism. These varied ORNs all project their axons along the ON and synapse with MTCs and interneurons in glomeruli in the OB (Gliem et al., 2013; Manzini et al., 2022; Nezlin & Schild, 2000). The OS of larval

*Xenopus laevis* comprises two prominent odour-processing streams (Gliem et al., 2013; Manzini et al., 2002). One stream is made of ORNs that project their axons in a lateral cluster of glomeruli in the OB and employ a cAMP-independent transduction cascade. These ORNs likely have a microvillous morphology and respond to amino acid odourants (Gliem et al., 2013; Manzini et al., 2002; Manzini, Heermann, et al., 2007; Manzini & Schild, 2010; Sansone et al., 2014). The second stream is made of ORNs that project their axons in a medial cluster of glomeruli in the OB and employ a cAMP-dependent transduction cascade. These ORNs likely have a ciliated morphology and primarily respond to odourants other than amino acids (Gliem et al., 2013; Manzini et al., 2002; Manzini, Heermann, et al., 2007; Manzini & Schild, 2010). A previous study (Hawkins et al., 2017) found that ON transection in larval *X. laevis* leads to the immediate death of all mature ORNs and increased proliferation of stem cells in the OE. Within 1 week after transection, new ORNs repopulate the OE and exhibit functional responses to odourants. These new ORNs begin to reconnect to the OB, where odourant-induced responses can be observed 3–7 weeks after transection. Although this suggests that the system has recovered by this point, it is yet unknown whether the recovered system is structurally and functionally equivalent to an unlesioned system. To tackle this question, in the present study, we first investigated whether the same spatially segregated odour-processing streams found in unlesioned larval *Xenopus* are also present in transected animals after recovery.

The OS must be able to detect and interpret individual odourants and combinations of multiple odourants (Buck, 1996; Grabe & Sachse, 2018; Manzini et al., 2022). Epithelial application of multiple odourants leads to the activation of distinct regions in the OB that are differentially tuned to the various odourants (Burton et al., 2022; Gliem et al., 2013; Johnson & Leon, 2007; Offner et al., 2023). To further investigate how accurately the *Xenopus* OS recovers its function after ON transection, in the present study, we identified and compared OB regions tuned to multiple different odourants in both unlesioned and recovered animals.

Whether the rewiring of the OS after a traumatic lesion, such as an ON transection, leads to a full recovery of function cannot be assessed only by measuring neural activity. To claim that rewiring leads to restored function, we must examine whether the rewiring restores odour-guided behaviour. For this reason, we further performed a set of odour-guided behavioural experiments to determine if and when, during the process of reinnervation after ON transection, larval *X. laevis* exhibit behavioural responses to odour stimuli, indicative of the full recovery of function of the OS. Behavioural responses are challenging to detect as little is known about how larval amphibians interpret specific odourant stimuli (Weiss, Manzini, & Hassenklöver, 2021). Therefore, we first developed an experimental protocol for detecting odour-guided behavioural responses in unlesioned *Xenopus* larvae. We then performed the same behavioural procedures and analyses with two groups of *Xenopus* larvae that had undergone ON transection—one group between 3 and 5 weeks of recovery and another group between 7 and 9 weeks of recovery.

Together, this study aimed to advance our understanding of the process of recovery of the OS after a severe injury. After bilaterally severing the ON, we found that the system quickly rewires, restoring its previous architectural structure. We show that this rewiring leads to the restoration of complex neural response patterns in the OB and the recovery of odour-guided behaviour. These results demonstrate that the rewired OS of *Xenopus* is de facto structurally and functionally equivalent to an unlesioned OS. Our findings thus showcase the remarkable neuroregenerative ability of this species and open up further avenues of investigation on the topic of neuroregeneration.

## 2 | MATERIAL AND METHODS

### 2.1 | Animal care

All *X. laevis* larvae used in this study were bred and kept in water tanks with constant water circulation at approximately 20°C at the animal facility of the University of Gießen. Before any invasive procedure, such as bulk electroporation of ORNs, ON transection or killing, *Xenopus* larvae were anaesthetised using 0.02% MS-222 (ethyl 3-aminobenzoate methanesulfonate; Sigma-Aldrich) dissolved in tap water. Developmental stages of *Xenopus* larvae were determined according to Nieuwkoop and Faber (Nieuwkoop & Faber, 1994), and all animals used were between stages 46 and 56 (both included). After developmental stage 56, major metamorphic remodelling of the OS begins to occur; therefore, animals past this stage of development were not used (Dittrich et al., 2016).

### 2.2 | Electroporation of ORNs and ON transection

For bulk electroporation of ORNs, we dissolved dried dye crystals of a fluorophore-coupled dextran (Cal 520 dextran conjugate, AAT Bioquest, 10 kDa, 3 mM) in frog Ringer's solution and applied it in the nostrils of anaesthetised

larvae (see above). We then applied six electric square pulses using two platinum electrodes (15 V, 25-ms duration at 2 Hz with alternating polarity) to each nostril (for detailed protocol, see Weiss et al., 2018). *Xenopus* larvae were then left to recover for at least 24 h before performing further experiments.

To transect the ON, we followed the same procedures previously developed (Hawkins et al., 2017). Briefly, *Xenopus* larvae were anaesthetised (see above) and placed under a binocular. Their nerves were then carefully severed at the mid-line of each nerve between the OE and the brain, using fine scissors to preserve surrounding tissue. After ON transection, the wound was closed with tissue adhesive (Histoacryl L; Braun). The larvae were then kept in tanks in the animal facility and used in further experiments at different time points during recovery from ON transection.

## 2.3 | Functional calcium imaging and image data processing

Functional calcium imaging experiments were performed on unlesioned *Xenopus* larvae and larvae at different time points after ON transection (non-transected animals; 3 weeks after ON transection; 7 weeks after ON transection). To perform calcium imaging experiments, ORNs were first loaded with a calcium-sensitive dye (Cal 520 dextran conjugate) via bulk electroporation, as described above. Animals were then anaesthetised (see above) and killed by severing the connection between the brainstem and the spinal cord. A tissue block containing the OS (the nose, the ONs and the rostral portion of the telencephalon, containing the OB; see Figure 1a) was carefully excised and kept in frog Ringer's solution to preserve tissue vitality. The ventral palatial tissue and a small portion of tissue surrounding the OE were removed to facilitate imaging and direct the flow of odourants into the nasal cavity. The tissue block was positioned in a recording chamber, held in place by a platinum grid with nylon strings and placed on the stage of a multiphoton microscope (Nikon A1R-MP). A constant flow of Ringer's solution across the tissue block was maintained throughout the experimental procedure. A perfusion manifold (Milli Manifold; ALA Scientific) connected to a multichannel gravity-fed perfusion system (ALA-VM-8 Series; Scientific) was placed directly in front of one nasal cavity, and the solution was removed from the opposing end of the recording chamber. Fast volumetric resonant scanning of the ORN axon terminals in the glomeruli of the OB was performed (780-nm excitation wavelength) as odourant stimuli were applied at different time intervals. This way, we created a time series of 3D virtual image stacks (axial dimensions: 180–300 μm, inter-plane distance 4 μm; lateral dimensions: 509 × 509 μm, 512 × 512 pixels), acquired at 0.5–1 Hz/image stack (for detailed information, see Offner et al., 2020). Stimuli used, shown in Table 1, were applied for 5 s each, with an interstimulus interval of 60 s. The application of these stimuli was repeated twice. Image analysis of 3D calcium image stacks and the estimation of odour-tuning profiles were performed using Python (version 3.9). The spatial distribution of response tuning profiles was analysed using Matlab (version R2019b). Motion artifacts were removed from images using a motion correction algorithm (Pnevmatikakis & Giovannucci, 2017). Denoised and deconvolved calcium imaging data was generated using the CaImAn toolkit (Friedrich et al., 2017; Giovannucci et al., 2019). Fluorescence intensity difference maps were created by calculating the difference between the peak fluorescence intensity of post-stimulus responses (averaged from three timeframes) and baseline fluorescence before stimulus onset (averaged from five frames). Note that fluorescence intensity difference maps were used to create maximum intensity projections along the *z*-axis shown in Figures 1 and 2. Individual timeframes had a duration between 1.5 and 2 s. The following criteria were used to define responding regions:

I. The area of regions had to be larger than 100 pixels.
II. Regions had to be responsive to at least one stimulus, that is, evoking a fluorescence intensity amplitude that exceeded the median value of all amplitudes in the dataset.
III. The deconvolved time series were compared to their corresponding raw traces as quality control.
IV. Any regions outside the boundaries of the glomerular clusters were discarded.

Fluorescence time traces of selected responding regions were baseline corrected using asymmetric least squares smoothing (Eilers & Boelens, 2005) and normalised by their response peak amplitude (baseline = 0, maximum = 1). A threshold of 12.5% was defined below which to ignore amplitude peaks within the expected peak response interval. Response tuning profiles of responding regions were therefore determined by the set of stimuli that led to response amplitudes above 12.5% of the maximum amplitude of the respective time series.

To analyse the spatial distributions of response tuning profiles in the OB, responsive regions were first sorted into forskolin-responsive and non-forskolin-responsive regions. Each subset was then further subcategorised based on responses to the used odourants. The size and position of each region within the glomerular clusters were determined in relation to manually defined points

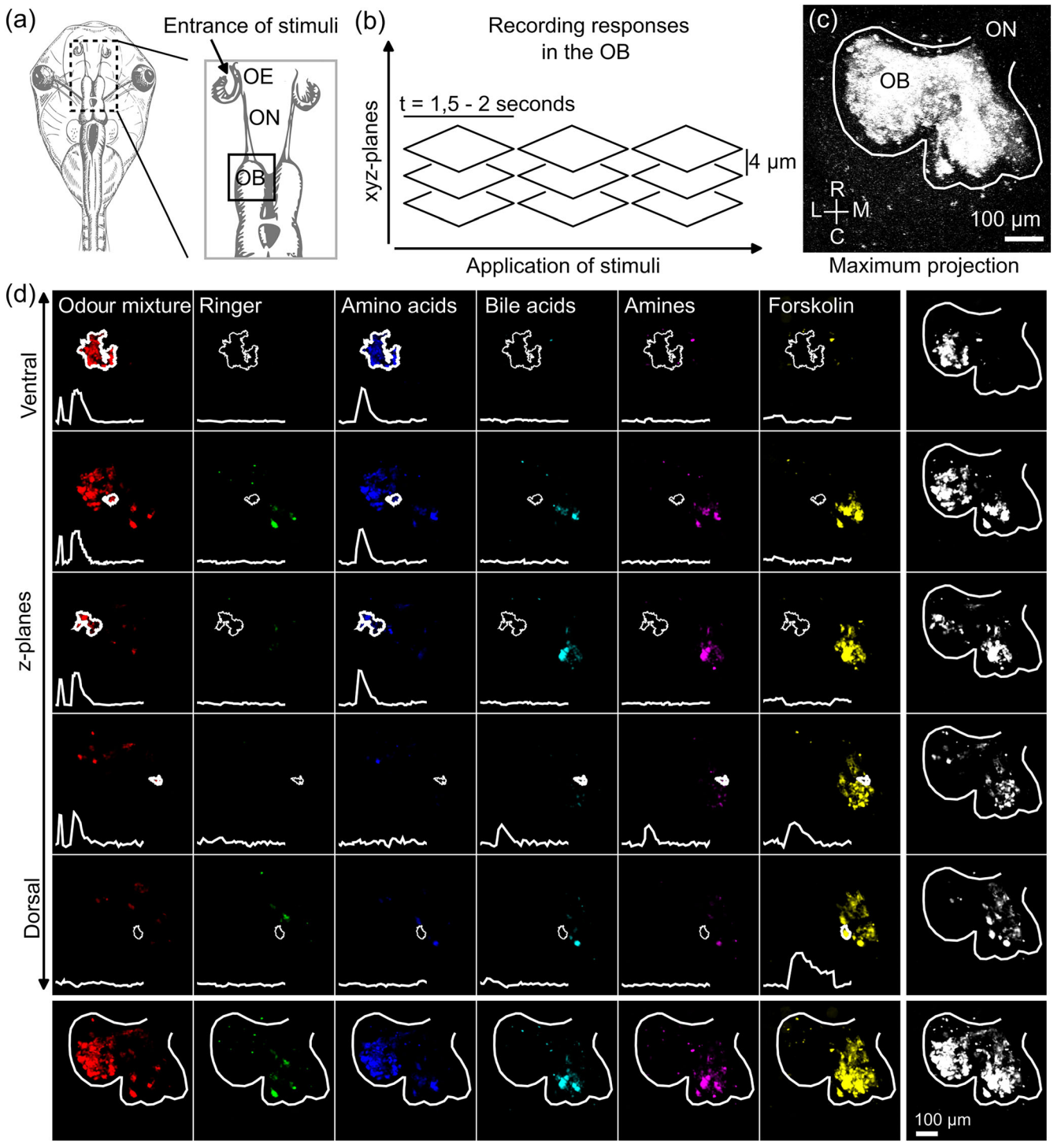


**FIGURE 1** Legend on next page.

at the medial–lateral and anterior–posterior edges of each OB. Along these two axes, the density of regions responsive to forskolin and non-forskolin-responsive regions was determined using Gaussian kernel density estimation. Kernel bandwidths were selected via Scott's rule (Scott, 1992; Virtanen et al., 2020). An overlap index $\eta$ was computed as the trapezoid rule integral of the overlap between these distributions (Pastore & Calcagnì, 2019).

## 2.4 | Odour-guided behaviour assay

Odour-guided behaviour experiments were performed on unlesioned *X. laevis* larvae and on larvae at different time points after ON transection. We tested non-transected *Xenopus* larvae, larvae that had recovered 3–5 weeks after ON transection and larvae that had recovered 7–9 weeks after ON transection. Before odour-guided behaviour experiments were performed, *Xenopus* larvae were kept for 24 h in individual tanks filled with regular tap water without food. After 24 h in this environment of reduced external stimuli, individual *Xenopus* larvae were placed in a partially separated choice tank filled with 1 L of regular tap water (see Figure 4). An infrared light panel was placed under the tank, and a camera was fixed above the tank at a distance that would allow recording of the position of the larvae in all regions of the tank. The choice tank was comprised of three regions, all freely accessible to the larvae – two separate 'areas of interest' of the tank of equal size (area = 58.5 $cm^2$) and a third, larger area (110 $cm^2$), used solely to allow the animal to enter and leave the areas of interest freely. Although the position of the larvae in this third region was recorded, these data were not used in any statistical analysis. After a habituation period of 2 h in which the larvae were left to swim freely in the tank without disturbances, we introduced simultaneously, through a gravity-fed perfusion system, 5 mL of an amino acid odourant mixture (each individual compound was diluted to a concentration of 100 μM in water; see Table 1), as an odour stimulus, to one area of interest of the tank, and 5 mL of regular tap water to the other (control stimulus). Stimuli entered the tank at a speed of 2 mL/min. In pilot testing, we released food colouring dye in the areas of interest of the tank through the gravity-fed perfusion system. We observed that the dye diffused beyond the regions of interest after approximately 20 minutes. Therefore, we set a 20-min exclusion threshold—data collected from animals that did not visit the areas of interest within the first 20 min after stimulus application were excluded from further analyses. This led to the exclusion of 20 out of 61 larvae tested. In control analyses, however, we verified that our results were robust to the exclusion threshold. Forty-one *Xenopus* larvae were included in the final analyses ($n = 18$, non-transected; $n = 10$, 3–5 weeks after ON transection; $n = 13$, 7–9 weeks after ON transection). These procedures were similar to those we previously employed (Weiss, Segoviano Arias, et al., 2021).

## 2.5 | Analyses of behavioural responses to odour stimuli in non-transected *Xenopus* larvae

Behaviour parameters were extrapolated from position tracking data using video tracking software (EthoVision XT, Noldus) and analysed using Matlab (version R2019b). These parameters were the percentage of time spent in each area of interest for each time period analysed (%), frequency of visits to each area of interest (visits/min), time spent in each area of interest per visit (s/visit) and

**FIGURE 1** Stimulus-induced responses of ORN axon terminals in the OB. **(a).** Illustration of a *Xenopus laevis* larva (view from top). The first two stages of the OS (highlighted by a dashed rectangular outline) are shown in a close-up to the right. It includes the nasal cavities lined by the OE, the ON and the OB. The arrow indicates the site of the stimulus application, and the rectangular outline indicates the location of the OB where calcium imaging was performed. **(b).** Simplified illustration of fast volumetric resonant scanning using a multiphoton microscope. Multiple *z*-plane stacks of the OB (one hemisphere) were obtained over time to identify 3D volumes within the OB exhibiting stimulus-induced fluorescence changes. **(c).** Example maximum projection image (raw data; Cal 520 fluorescence) of responsive ORN axon terminal regions in the OB (one hemisphere; outlined in white) of a non-transected animal. All responses to stimuli (odourants and forskolin; see Table 1) applied are overlayed and shown in white. **(d).** Example maximum projection images (difference maps) of *z*-plane bundles of the OB of the same animal as shown in **(c)**. *z*-plane bundles are distributed from most ventral to most dorsal (top to bottom) and over the time of stimuli application (left to right). This visualisation shows the location and temporal activation pattern of example responsive regions in the OB (randomly selected for illustrative purposes). Overlays of all responsive regions over time for each *z*-plane bundle are shown in white at the far right. Overlays of all ventral to dorsal regions responsive to each stimulus are shown in the bottom line of the images. In all overlay figures, the outline of the OB is shown for reference. Raw traces of odor response profiles (Cal 520 fluorescence) are included (white traces as inlays) for specific responsive regions (outlined in white) in each *z*-plane bundle. Similar results were obtained in four different animals (one hemisphere/animal). C, caudal; OB, olfactory bulb; OE, olfactory epithelium; ON, olfactory nerve; L, lateral; M, medial; R, rostral.

**TABLE 1** Composition and concentration of stimuli applied to the OE during calcium imaging recordings and behavioural experiments.

| Stimuli | Composition |
|---|---|
| Amino acid mixture | L-valine, L-leucine, L-isoleucine, L-methionine, glycine, L-serine, L-threonine, L-cysteine, L-arginine, L-lysine, L-histidine, L-tryptophan, L-phenylalanine, L-alanine, L-proline (100 μM in frog Ringer's solution) |
| Amine mixture | 2-phenylethylamine, tyramine, butylamine, cyclohexylamine, hexylamine, 3-methylbutylamine, N,N-dimethylethylamine, 2-methylbutylamine, 1-formylpiperidine, 2-methylpiperdine, N-ethylcyclohexylamine, 1-ethyylpiperidine, piperidine (100 μM in frog Ringer's solution) |
| Bile acid mixture | Taurocholic acid, cholic acid, glycholic acid, deoxycholic acid (100 μM in frog Ringer's solution) |
| Forskolin | Forskolin [activates the enzyme adenylate cyclase, thereby increasing the concentration of cAMP; (100 μM in frog Ringer's solution)] |

*Note*: Alongside these stimuli, a positive control made of all stimuli (with the exception of forskolin, L-proline and L-alanine; 50 μM in frog Ringer's solution; also see Gliem et al., 2013) and a negative control made solely of frog Ringer's solution was applied. All chemicals were purchased from Sigma Aldrich. Amino acids, bile acids and amines were selected as odourant stimuli as they are water-soluble molecules and are known to be olfactory stimuli for aquatic animals (amino acids: Caprio & Byrd, 1984; Gliem et al., 2013; Kang & Caprio, 1995; Manzini et al., 2002; Manzini & Schild, 2003, 2004; Schild & Manzini, 2004; bile acids: Gliem et al., 2013; Kang & Caprio, 1995; Sato & Suzuki, 2001; amines: Carr et al., 1990; Carr & Derby, 1986; Gliem et al., 2009; Rolen et al., 2003).

swimming velocity in each area of interest (cm/s). Each parameter was measured during the 2-h habituation period and over the course of 5, 10, 20, 40 and 60 min, starting from the first entry of larvae in each area of interest after stimuli application.

The average parameter values measured during the 2-h habituation period, where no stimuli were applied, were used as the baseline for comparison to values obtained after stimulus application. For each parameter recorded after applying stimuli, we computed the absolute value of the parameter's change from the baseline. To obtain a single value describing the change in behaviour from baseline, we first fit the data with a log parabolic function in the form: $f(x) = \log(ax^2 + bx + c)$. Then, we took the area under the curve (*AUC*) of the fitted function, normalised to the measurement duration, as a metric of change in behaviour from baseline. Figure 4d exemplifies this sequence of computations for two examples of non-transected *Xenopus* larvae.

In non-transected larval *Xenopus*, behavioural variables were compared across areas of interest during the 2-h habituation period to exclude any differences between these areas at baseline. Then, *AUC* values computed for each parameter were compared across areas of interest to identify which parameters showed a greater change from baseline in the area of interest where amino acid odourants had been applied compared to the area of interest where normal tap water had been applied. After identifying which behaviour parameters signalled statistically significant responses to the odourant stimulus, we computed a robust metric of behavioural response. We defined, for each parameter, an odourant response index (*ORI*) as a ratio of the absolute change in behaviour in the amino acid compartment ($AUC_{aa}$) minus the absolute change in behaviour in the water compartment ($AUC_w$), divided by the absolute change in behaviour in the water compartment:

$$ORI = \sqrt[3]{\frac{AUC_{aa} - AUC_w}{AUC_w}}.$$

The cube root transformation was applied to remove the skewness in these proportion data. Positive (>0) values of this *ORI* indicate a behavioural response. We then combined the *ORI* of parameters (time per visit and swimming velocity) that showed a significant behavioural response by taking their average. This combined *ORI* was taken as a robust metric of behavioural response to odourant stimuli.

## 2.6 | Analyses of behavioural responses to odour stimuli in transected *Xenopus* larvae

The previous analyses determined which parameters showed significant behavioural responses to odour stimuli in non-transected *Xenopus* larvae. These parameters were then employed, using the same set of analyses, to test for the recovery of odour-guided behaviour in *Xenopus* larvae during different periods of recovery from ON transection. Specifically, in larvae between 3–5 and 7–9 weeks after ON transection, we compared the *AUC* values for time per visit and swimming velocity parameters across areas of interest to test whether these parameters showed a greater change from baseline in the area of interest where amino acids had been applied. We then computed the *ORI* for both parameters, as well as the combined *ORI*, and tested whether these indexes signalled behavioural responses to the odour stimuli in the two groups of transected *Xenopus* larvae.

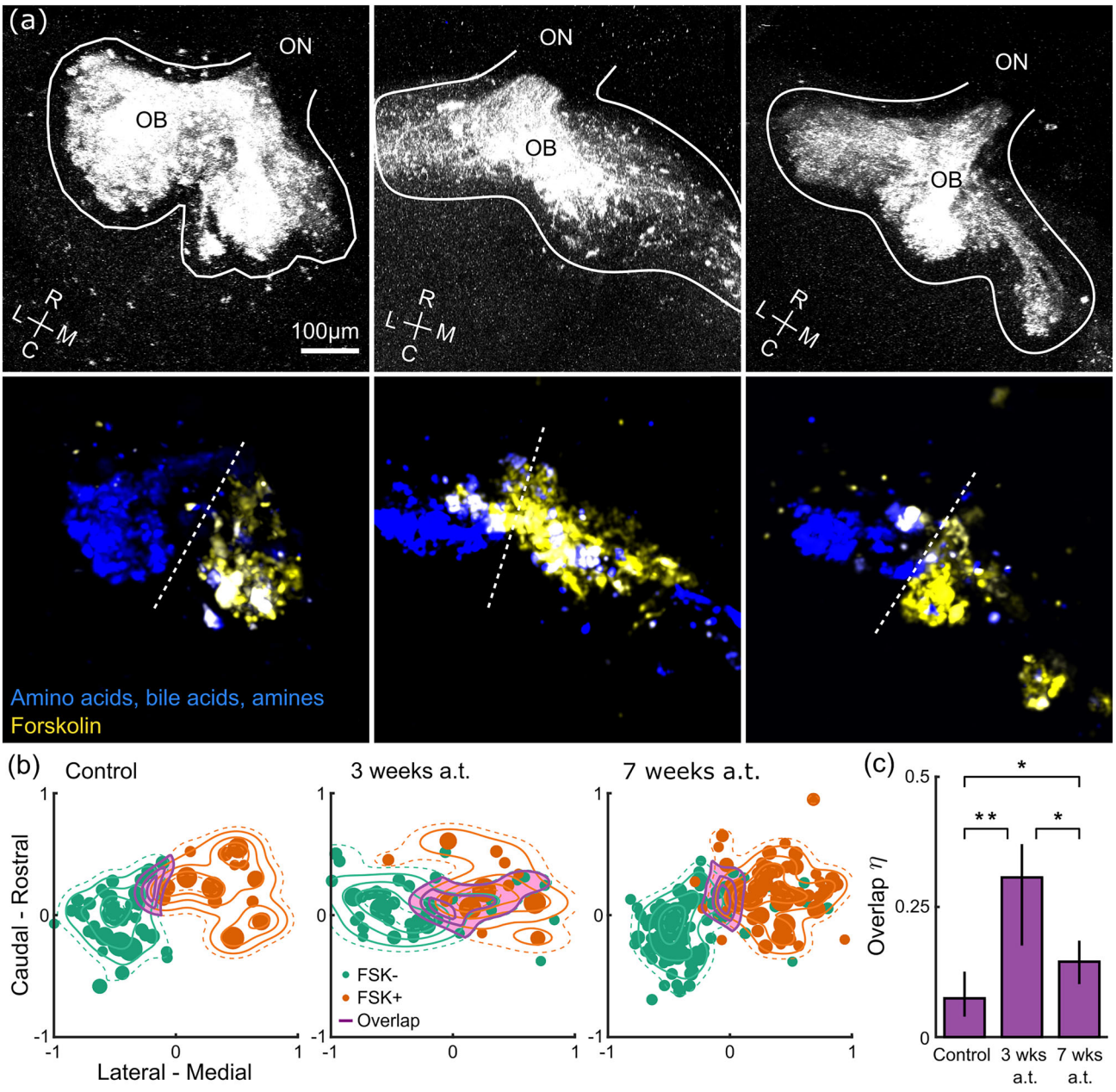


**FIGURE 2** Spatially and functionally distinct odor streams are reformed during OS regeneration after ON transection. **(a).** Maximum projection images of the OB of three representative animals: the left panels show data from one non-transected larval *Xenopus*, and the middle and right panels show data from animals at three and 7 weeks of recovery after ON transection. Images in the top panels (raw data; Cal 520 fluorescence) show all regions in the OB that responded to the applied stimuli (in white). Lower panels (corresponding difference maps) show responses to all odor mixtures (blue) and forskolin (yellow). Overlapping responsive regions are visible as white areas. The dashed lines indicate the midline of the OB. **(b).** Density plots showing the spatial distribution of regions responsive exclusively to forskolin (FSK+; orange) and regions responsive to odourants but not to forskolin (FSK−; blue) along lateral to medial and caudal to rostral axes for *Xenopus* larvae before ($n = 4$ animals) and at three ($n = 4$ animals) and 7 weeks ($n = 10$ animals) after ON transection (shown from right to left). Individual responsive regions collected from each larval *Xenopus* are shown as dots in the respective colours. The dot size is proportional to the region size. The overlap of FSK+ and FSK− distributions is shown in purple. **(c).** Overlap index $\eta$ of forskolin-only and forskolin-negative distributions throughout recovery from lesion. The overlap index $\eta$ is estimated as the volume under the overlap surfaces. Statistical significance and 95% confidence intervals were obtained through a bootstrapping procedure. a.t., after transection; C, caudal; FSK +, regions responsive exclusively to forskolin; FSK−, regions responsive to odourants but not to forskolin; OB, olfactory bulb; ON, olfactory nerve; L, lateral; M, medial; R, rostral; wks, weeks. $^{*}p < .05$; $^{**}p < .01$.

### 2.7 | Statistical analysis

A bootstrapping procedure was employed for calcium imaging analyses to assess whether the overlap index was statistically different in transected and non-transected *X. laevis* larvae. Overlap indices in each group were computed from the original data resampled with replacement 1000 times. These bootstrapped distributions were used to compute the 95% confidence intervals of the overlap index estimates. The differences between the bootstrapped distributions were then fit to Gaussian cumulative distribution functions to compute p-values. Overlap indices across groups that fell outside the bounds of each other's confidence intervals (corresponding to $p < .05$) were considered to be significantly different.

Differences between groups were assessed using one- or two-tailed Wilcoxon signed-rank or rank-sum test tests, as appropriate. The Pearson correlation coefficient was employed to assess the degree of linear dependency between behavioural parameters. Statistical significance was set at $\alpha < .05$.

## 3 | RESULTS

### 3.1 | Stimulus-induced activity of ORN axon terminals within the OB

We performed fast volumetric calcium imaging to record odourant- and forskolin-induced activity of ORN axon terminals in the glomerular layer of the OB (see Figure 1a,b) to better characterise the two previously identified odour-processing streams present in the OS of larval *X. laevis* [see (Gliem et al., 2013; Manzini et al., 2002) and Introduction]. In particular, we wanted to precisely locate distinct odourant- and forskolin-responsive regions in the ventral–dorsal and lateral–medial axes of the OB. Figure 1c shows a maximum projection of ORN axon terminal activity (shown in white) in response to the epithelial application of odourant mixtures and forskolin (see Table 1). Figure 1d shows the same OB deconstructed into regions responsive to individual odourant mixtures and forskolin (from left to right) and at different levels across the ventral–dorsal axis of the OB (top to bottom). Responses to amino acids (third column, blue) occur predominantly in ventral–lateral areas of the OB, whereas responses to forskolin (sixth column, yellow) occur in dorsal–medial regions. Responses to bile acids and amines (fourth and fifth column, cyan and magenta) occur in intermediate–medial regions of the OB. The different responsive regions can respond to a single odourant mixture or multiple odourant mixtures. Numerous regions are solely responsive to forskolin, but we also found forskolin-responsive regions that react to odourant mixtures (primarily to amines and bile acids). Each region can thus be defined by its OB location and response profile. Examples of stimulus-induced response profiles of specific axon terminal regions (outlined in white) are included as raw data traces at the bottom of each sub-panel (inlays in white). This set of experiments functionally characterised the two prominent and largely separated regions of the OB of non-transected control larvae. Similar results were obtained in four different animals (one hemisphere/animal).

### 3.2 | Regenerating ORN axons reestablish functional odour processing streams in the OB after ON transection

Fast volumetric calcium imaging of the OB was performed on non-transected *Xenopus* larvae and larvae that had recovered for different periods after ON transection, allowing us to detect odourant- and forskolin-induced activity of ORN axon terminal regions throughout the OB. Representative images of odourant- and forskolin-induced activity in the OB of a non-transected animal and in two animals 3 and 7 weeks after ON transection, respectively, are shown in Figure 2a (top row). The obtained results suggest that a substantial amount of functional reinnervation of the OB by new ORNs has already occurred after 3 weeks of recovery from ON transection. By categorising the OB activity (corresponding example difference maps are shown in Figure 2a, bottom row) in response to the epithelial application of the odourant mixture (blue) and in response to the application of forskolin (yellow), we observed that some anatomical segregation of ORN axon terminals that respond to these different stimuli is visible in both non-transected *Xenopus* larvae and transected and recovered larvae. Note that overlapping responsive regions are visible as white areas. Next, we quantified this observation at the group level across all imaged animals.

From the calcium imaging data acquired, we identified and examined individual, specialised regions within the OB of the larvae. A 'region' was defined as a group of adjacent voxels responding to the same stimuli combination, that is, exhibiting the same odourant/stimulus tuning profile. Each region was thus distinguished by its specific tuning profile and 3D spatial location in the OB. In non-transected *Xenopus* larvae, 86 responsive regions with distinct spatial locations were found ($n = 4$ animals, one hemisphere/animal—average of 21.5

regions/hemisphere). In animals that had recovered for 3 weeks after ON transection, 82 responsive regions with distinct anatomical locations were found ($n = 4$ animals, one hemisphere/ animal—20.5 regions/hemisphere). In animals that had recovered for 7 weeks after ON transection, 267 responsive regions with distinct anatomical locations were found ($n = 10$ animals, one hemisphere/ animal—26.7 regions/hemisphere). Regions varied widely in size across the different groups. In non-transected *Xenopus* larvae, the size of responsive regions (mean ± standard deviation) was 1400.95 ± 1991.61 $\mu m^2$. After 3 weeks of recovery from ON transection, the size of responsive regions was 900.21 ± 1719.08 $\mu m^2$, which was significantly smaller than in non-transected larvae ($p < .001$). Seven weeks after recovery, the size of responsive regions was 958.36 ± 1641.40 $\mu m^2$, which was significantly smaller than in non-transected larvae ($p < .001$) but not significantly different than at 3 weeks ($p = .40$).

Having identified these responsive regions, we employed them to quantify the extent to which the two anatomically and functionally segregated odour processing streams present in larval *Xenopus* (see Introduction and Gliem et al., 2013) are reestablished during the process of ORN reinnervation of the OB after ON transection. Specifically, we estimated the probability density function of these regions along two spatial axes. Figure 2b shows the spatial distribution of axon terminal regions responsive exclusively to forskolin (orange; cAMP-dependent) and axon terminal regions responsive to odourants but not forskolin (teal; cAMP-independent) along the medial–lateral and anterior–posterior axis for all time points (before and after ON transection). In non-transected *Xenopus* larvae, regions responding to forskolin and innervated by ORNs with cAMP-dependent transduction cascade were generally distributed more medially and rostrally ($n = 4$ animals). Regions that responded to odourants but not forskolin were distributed laterally and caudally ($n = 4$ animals). In larvae that recovered for 3 weeks after ON transection, although some distinction is already visible, there is significantly more overlap between forskolin-responsive and non-responsive regions (Figure 2c; $p = .0014$; $n = 4$ animals). At 7 weeks after transection, the spatial and functional distributions recover substantially, and the overlap between forskolin-responsive and non-responsive regions is significantly less than at 3 weeks ($p = .019$; $n = 10$ animals). However, it remains slightly greater than in non-transected *Xenopus* larvae ($p = .047$). These results thus demonstrate the progressive re-establishment of the spatially segregated cAMP-dependent and cAMP-independent odour processing streams in the OB during reinnervation of the OB by newly formed ORNs after ON transection.

### 3.3 | OB regions with multi-stimulus response tuning profiles are reestablished during recovery from ON transection

To further investigate the accuracy of the re-establishment of the olfactory network after ON transection, we analysed in detail the specific odourant and forskolin tuning profiles of different responsive axon terminal regions in the OB (same set of experiments as used for Figure 2b). Across all non-transected and transected *Xenopus* larvae, we found 15 distinct regions with characteristic tuning profiles corresponding to all possible combinations of the applied stimuli (positive and negative controls excluded; Figure 3). The most common response profile across all animals showed responses solely to amino acid odourants (Figure 3a). The second most common response profile in non-transected larvae and larvae 7 weeks after ON transection showed responses solely to forskolin. The response profile that showed activity solely to forskolin was the third most common profile in larvae 3 weeks after ON transection. We also found large proportions of regions exhibiting responses to combinations of stimuli. For example, the third most common profile in non-transected larvae and the fourth most common profile in larvae 7 weeks after transection was that of regions responding to both amines and forskolin.

By looking at the percentage of regions exhibiting each of the 15 distinct tuning profiles (Figure 3b), we observed that all 15 response profiles were present in non-transected animals. Conversely, only 12 of these 15 response profiles were found in larvae 3 weeks after ON transection. Specifically, in larvae 3 weeks after ON transection, no regions responded exclusively to amines, bile acids and amines or amino acids and bile acids and amines. All 15 odour response profiles found in non-transected larvae, albeit with a slightly different frequency, were again found in larvae 7 weeks after ON transection (Figure 3b).

The results shown in Figures 2 and 3 highlight how the transmission of information from the OE to the glomeruli in the OB is reestablished following ON transection and indicates that this rewiring reliably reestablishes the olfactory network as before transection. Nevertheless, this does not answer whether reestablishing the wiring structure is sufficient to recover odour-guided behaviour after ON transection. To establish whether and when this is the case, we developed and executed experiments investigating odour-guided behaviour using amino acids as olfactory stimuli.

### 3.4 | Defining odourant-guided behavioural responses in larval *X. laevis*

To investigate odourant-guided behaviour, we performed experiments to track the 2D position of individual *X. laevis* larvae in a partially separated choice tank (Figure 4a). During a 2-h habituation period, in which no odourants were applied to the choice tank, freely swimming larvae explored the whole volume of the tank (Figure 4a). The example tadpole shown in Figure 4a exhibits a preference for wall following, a typical behaviour previously described in the literature (e.g., Hänzi & Straka, 2018). From the motion tracking data acquired in the two areas of interest of the tank (areas A and B), we extracted four parameters: (i) the percent of time spent in each area, (ii) the frequency of visits per minute, (iii) the time spent per visit in seconds and (iv) the swimming velocity in centimetres per second.

As expected, during the 2-h habituation period without odour stimulation, we found no significant differences between the two areas of interest for any of these four parameters (Figure 4b, all $p > .05$). Across areas of interest and animals ($n = 18$), the average percentage of time spent per area was $20 \pm 8\%$ (mean ± standard deviation), the average frequency of visits to each compartment was $0.8 \pm 0.5$ visits/min, the average time per visit was $25 \pm 25$ s and the average swimming velocity was $1.1 \pm 0.6$ cm/s. Additionally, these parameters were all significantly correlated across animals and measurement time points (all $p < .05$), with the strongest correlation being between time per visit and velocity parameters ($r = -0.52$, $p < .001$). These results suggest that these parameters capture common sources of variance in the animals' behaviour. For example, the negative correlation between time per visit and velocity parameters sensibly indicates that when *Xenopus* larvae swam at slow speeds, they also tended to remain in the same portion of the tank for longer.

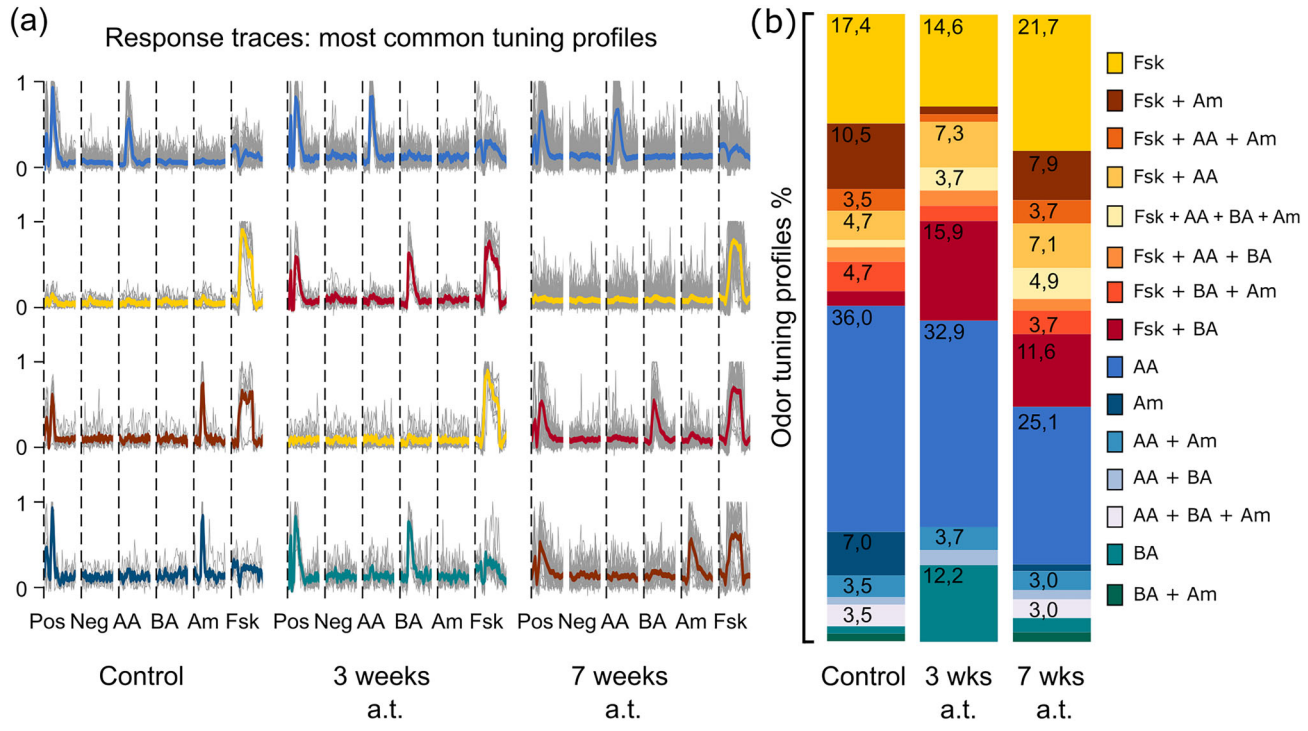


**FIGURE 3** Tuning profiles of ORN axon terminal regions in the OB before and during recovery from ON transection. **(a).** Odourant/stimulus–response profiles found in the OB of *Xenopus laevis* larvae. The left, middle and right columns respectively show profiles found in all non-transected animals, animals 3 weeks after ON transection and animals 7 weeks after transection. From top to bottom, we show the four most common profiles found in each group (positive and negative controls excluded). Normalised response profiles of individual regions are shown as grey traces. Average traces plotted as overlays follow the colour code indicated in (b). **(b).** Percent of ORN axon terminal regions exhibiting different odourant/stimuli-induced tuning profiles in the OB of all non-transected animals (left column) and larvae 3 weeks (middle column) and 7 weeks (right column) after ON transection. Numbers are shown as percentages of the total number of regions found—non-transected larvae ($n = 4$ animals, one hemisphere/animal, total of 86 responsive regions), 3 weeks post-transection ($n = 4$ animals, one hemisphere/animal, total of 82 responsive regions), 7 weeks post-transection ($n = 10$ animals, one hemisphere/animal, 267 responsive regions). AA, amino acids; Am, amines; a.t., after transection; BA, bile acids; Fsk, forskolin; Neg, negative control; Pos, positive control; wks, weeks.

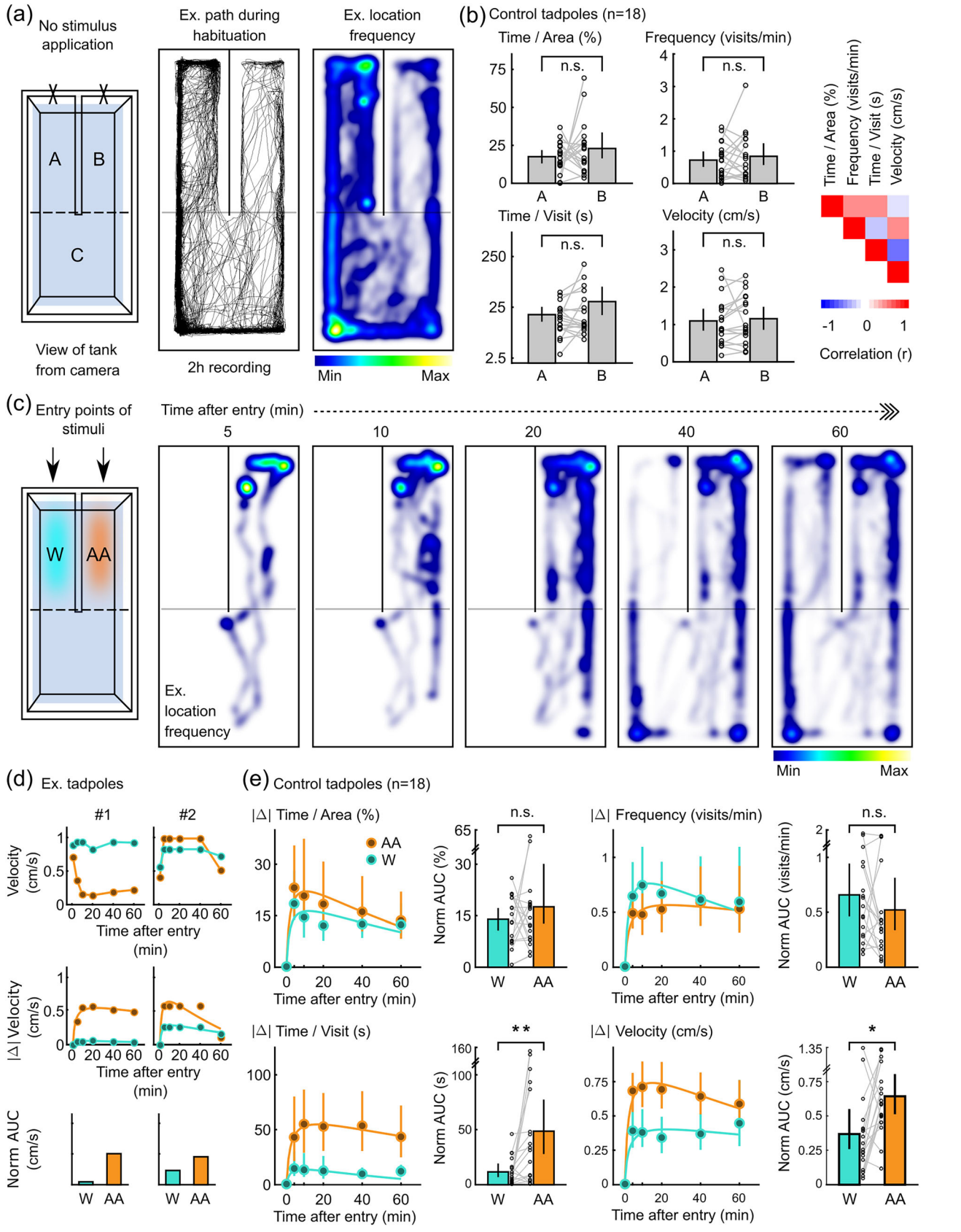


**FIGURE 4** Legend on next page.

Having established that there were no intrinsic differences in the behaviour of larval *Xenopus* within the two areas of interest of the tank, we next proceeded to identify odour-guided behavioural responses. At the end of the 2-h habituation period, a mixture of amino acid odourants was applied to one of the areas (AA area) while water, as a control, was applied to the other area (W area, Figure 4c). The odour stimulus was the same mixture of amino acids used in the calcium imaging experiments described above. The *Xenopus* larvae continued to swim freely in the tank for 60 minutes while we tracked their movements (Figure 4c). To detect a behavioural response to the odour stimuli, we monitored how each behavioural parameter extracted from the movement traces varied compared to baseline, that is, the average parameter value during the 2-h habituation period.

Amino acids are known to be olfactory stimuli for aquatic animals (e.g., Caprio & Byrd, 1984; Kang & Caprio, 1995; Manzini et al., 2002; Manzini & Schild, 2003, 2004, 2010; Schild & Manzini, 2004). However, it is unknown what these stimuli signify to *Xenopus* larvae. For example, these stimuli could signal food sources and/or the presence of predators and lead to complex and even dichotomous response behaviours (e.g., De Franceschi et al., 2016). For this reason, we expected that changes in value for each parameter, signaling a change in behaviour, could occur as an increase or decrease from the baseline. Figure 4d shows data on the swimming velocity of two example larvae (non-transected). Tadpole #1 shows a reduction in swimming velocity after the first entry in the AA area, whereas the swimming velocity in the area where water was applied shows no apparent change. Tadpole #2 exhibits an increase in swimming velocity in both areas, and this increase is greater in the AA area (Figure 4d, top panels). To obtain a single value describing the change in behaviour from baseline, we took the absolute value of the change from baseline, and we fit these data with log parabolic functions (Figure 4d, middle panels). Then, we took the area under the curve (AUC) of these fitted functions, normalised to the measurement duration, as our metric of change in behaviour from baseline (Figure 4d, bottom panels). The change in behaviour from baseline in the water compartment (blue) represents random changes in each animal's behaviour with time. Any additional change in behaviour in the AA area (orange) should be attributable to the animals detecting the odourant stimulus in the water.

We applied this method across all animals for each of the four parameters extracted from the movement traces (Figure 4e). We did not find statistically significant differences between the AA and W areas regarding the percentage of time spent per area ($p = .45$) or the frequency of visits per area ($p = .96$). Conversely, we found that behaviour in the AA area was significantly different than in the W area with respect to the time per visit

**FIGURE 4** Motion and behaviour tracking without and with added odor stimuli in non-transected *Xenopus* larvae. **(a).** Schematic of the partially separated choice tank (as seen from the camera; top), followed by raw movement traces, and the spatial distribution of explored tank locations for one representative larva during a 2-h habituation period where no odor stimulus was applied. Areas A and B were the areas of interest from which motion-tracking data were collected and analysed. Area C was a compartment connecting the two areas of interest so that *Xenopus* larvae could freely move between areas A and B or retreat from both. Motion tracking data from area C was not analysed. **(b).** Behavioral parameters extracted from the motion tracking data during the 2-h habituation period in compartments A and B (no odor stimulus applied) for all animals ($n = 18$) and correlation map. Bars are means, and error bars are 95% bootstrapped confidence intervals. Connected dots represent data from individual larvae. All paired comparisons $p > .05$. The strength of the correlations between the four parameters was extracted from the motion tracking data from all animals (all $p < .0001$). **(c).** Illustration of the partially separated choice tank as seen from the camera. An amino acid odourant mixture (AA) and water (W) were simultaneously introduced via gravity feed into two separate locations of the choice tank (AA and W areas). Arrows show where the stimuli were introduced in the two areas of interest in the tank. The two areas of interest end at the dashed line. Behavioral parameters were extracted from motion tracking data recorded within these two areas of interest. Location frequency for one representative tadpole is shown at different time points after the first entry in AA and W areas. **(d).** For two representative animals, the top plots show swimming velocity in the areas of the tank where we introduced AA (orange) and W (blue) at baseline (t = 0) and as a function of time since the first entry in each area of interest. Tadpole #1 exhibits a decrease in velocity in the AA area, whereas tadpole #2 exhibits an increase in velocity in the AA area. Middle plots show the absolute value of the change in velocity from baseline as a function of time from the first entry in the AA and W areas. Curves are log parabolic functions fit to the data. In the rightmost plots, the change in behaviour from baseline was computed as the normalised area under the curve (AUC) of the fitted log parabolic functions. AUC data show that both *Xenopus* larvae exhibited a greater change in velocity in the AA areas, even though this change was in different directions for the two larvae. **(e).** For each of the four measured parameters, the left plots show the absolute value of the change from baseline as a function of time from the first entry in the AA (orange) or W (blue) areas. Dots are means across larvae; error bars are 95% bootstrapped confidence intervals of the mean. Lines are the average best-fitting log parabolic functions through the data. Corresponding right plots show the change in behaviour from baseline computed as the normalised area under the curve (AUC) of the fitted log parabolic functions (small connected dots represent values for individual larvae). AA, amino acids; n.s., not significant; W, water. $^{*}p < .05$; $^{**}p < .01$.

($p = .0035$) and the velocity parameters ($p = .016$). In the AA area, *Xenopus* larvae modified their behaviour by changing how quickly they swam and how much time they spent in the AA area during each visit. These two parameters were also moderately correlated (as described above; Figure 4b). These results suggest it should be possible to combine these parameters into a single, robust index of behavioural response to the amino acid stimuli.

### 3.5 | Recovery of established odour-guided behaviour parameters in larval *X. laevis* after ON transection

Having determined which parameters reflect odour-guided behavioural responses in non-transected *Xenopus* larvae, we used these parameters to test whether lesioned animals would recover such odour-guided behavioural responses. We repeated the same experiments previously performed on unlesioned animals with animals at different time points during recovery from ON transection.

We found no evidence of behavioural response to odourant stimuli in *Xenopus* larvae that had recovered 3–5 weeks after ON transection ($n = 10$ animals; Figure 5a). We did not find statistically significant differences between the AA and W areas in terms of time per visit ($p = .54$) or velocity ($p = .28$). However, the situation differed for animals that had recovered 7–9 weeks after ON transection ($n = 13$ animals; Figure 5b). In this group, we found statistically significant differences between the AA and W areas in terms of time per visit ($p = .016$) and velocity ($p = .047$).

To combine these two parameters into a single robust index of behavioural response to the amino acid odourants, each parameter was first defined as a unitless odourant response index (ORI, see Methods for precise mathematical formulations). Values of these indices around zero signify that no odour-induced change in behaviour is detected. Figure 5c concisely summarises our behavioural results across non-transected and transected animals using the combined time–velocity odourant response index. The combined ORI was significantly greater than zero and thus detected odour-guided behavioural responses in non-transected *Xenopus* larvae ($p < .001$; $n = 18$ animals) and in larvae that had recovered 7–9 weeks after ON transection ($p = .0085$; $n = 13$ animals but not in larvae that had recovered 3–5 weeks after ON transection ($p = .31$; $n = 10$ animals).

These results indicate that ORN axon rewiring after ON transection in larval *X. laevis* reliably reestablishes the olfactory network to the degree that allows for odour perception.

## 4 | DISCUSSION

Despite various phylogenetic adaptations, the OS maintains similar functional and structural features across vertebrates (Ache & Young, 2005; Eisthen, 2002; Manzini et al., 2022; Poncelet & Shimeld, 2020). The OE comprises supporting cells, ORNs and a stem cell niche that maintains the epithelial cell population (Brann & Firestein, 2014; Manzini et al., 2022). The axons of ORNs connect to the OB, where they form synaptic connections with MTCs and interneurons. After various processing steps within the OB, the olfactory information is relayed to higher brain centres by MTCs (Manzini et al., 2022). A stem cell niche is also present in the subventricular zone in the central nervous system, from where neuroblasts migrate to the OB via the rostral migratory stream to replenish bulbar interneurons (Lledo & Valley, 2016; Manzini et al., 2022; Tufo et al., 2022). Maintenance of stem cell niches that can replace OE and OB neurons throughout life results in a remarkable regenerative capacity of the OS (Brann & Firestein, 2014; Lim & Alvarez-Buylla, 2016; Schwob et al., 2017). However, the extent, time course and accuracy of recovery from injury depend on the species, developmental stage, age and the extent and location of the injury (Calvo-Ochoa et al., 2021; Hawkins et al., 2017; Schwob, 2002; Schwob et al., 2017, and references therein). The human OS also regenerates after damage to the OE or the central olfactory processing pathways (Whitcroft et al., 2023). In humans, head traumas are one of the leading causes of olfactory dysfunction (Frasnelli et al., 2016). Such injuries can be accompanied by a complete and permanent loss of the sense of smell if the trauma entirely severs the ONs. Despite intensive research, no reliable treatments have yet been found that lead to the restoration of the sense of smell in humans (Jafari & Holbrook, 2022). Researching and understanding the basic physiological mechanisms that support OS regeneration in vertebrates is therefore essential to develop necessary treatments.

In a previous study, we monitored the time course of rewiring of the OS of larval *X. laevis*, an anuran amphibian, after ON transection (Hawkins et al., 2017). In the present study, using functional calcium imaging and behavioural tests, we show that the *Xenopus* OS rewires with extremely high accuracy.

### 4.1 | Localisation of odour-processing streams in the OB and recording of odourant- and forskolin-induced responses in ORN axon terminal regions

The main OS of larval *X. laevis* has long been known to include two anatomically and functionally segregated

odour-processing streams (see Introduction and Weiss, Manzini, & Hassenklöver, 2021). Identical odour-processing streams are also present in the *Xenopus* postmetamorphotic OS specialised to detect water-borne olfactory stimuli (Nakamuta et al., 2011; Weiss, Segoviano Arias, et al., 2021), and similar streams are also present in the OS of fishes (Olivares & Schmachtenberg, 2019; Sato et al., 2005).

Here, we performed odourant- and forskolin-induced calcium imaging within the whole volume of the glomerular layer of the OB of non-transected *X. laevis* larvae to better localise and further investigate these streams (see Figure 1). The lateral glomeruli innervated by ORNs of the lateral stream are located more ventrally and caudally in the OB. In contrast, the medial glomeruli innervated by ORNs of the medial stream have a more dorsal and rostral location. We found that within the 3D volume of the OB, only minimal spatial overlap exists between the projection areas of the two streams.

We next identified 15 distinct bulbar regions with characteristic tuning profiles corresponding to all combinations of the applied stimuli (odourants and forskolin; see Table 1). The most frequently identified regions were exclusively responsive to amino acid odourants (36%). In addition, approximately 20% of the responsive regions responded to amino acids and combinations of other odourants (bile acids and amines) and/or forskolin. Of these, 12% responded to amino acids and forskolin. The second most frequently identified regions responded solely to forskolin (17.4%). In addition, 29% of the responsive regions responded to forskolin and combinations of the other odourants; 7% of the responsive regions responded solely to amines and about 1% solely to bile acids. The vast majority of responsive regions responded to one odourant group, but some regions responded to two or three odourant groups. These results are substantially in agreement with previous results from our group, in which we recorded tuning profiles to odourants and forskolin of individual ORNs (Czesnik et al., 2006; Gliem et al., 2009, 2013; Manzini et al., 2002; Manzini & Schild, 2003; Weiss, Segoviano Arias, et al., 2021), glomeruli (Gliem et al., 2013; Manzini, Brase, et al., 2007; Manzini, Heermann, et al., 2007) and bulbar neurons (Manzini et al., 2002; Weiss, Segoviano Arias, et al., 2021).

Building on these detailed data, we investigated how precisely the OB network functionally regenerates after ON transection.

## 4.2 | Precise functional regeneration of the peripheral OS is completed 7 weeks after transection of the ON

In a previous study, we found that during recovery from ON transection, ORNs reestablish synaptic connections in the OB and that glomeruli and OB neurons again start responding to odourants within three and 7 weeks (Hawkins et al., 2017). We did, however, not assess how precise the functional rewiring of the system is. In the present study, we set out to answer this question by performing odourant- and forskolin-induced calcium imaging within the whole volume of the glomerular layer of the OB of *X. laevis* larvae three and 7 weeks after ON transection.

Three weeks after ON transection, axons of newly formed ORNs of both odour streams, with cAMP-dependent and cAMP-independent transduction mechanisms, reached the OB and responses to both odourants and forskolin started to reappear in the OB. However, the terminal regions of the two odour streams still had a significantly higher spatial overlap than control (non-transected) larvae (see Figure 2). This observation is in line with the results of our previous study, in which we saw that 2–3 weeks after ON transection, many aberrant ORN axons were still present in the OB, and the characteristic cluster structure of glomeruli had not yet fully recovered (Hawkins et al., 2017). In other vertebrate species, it has been shown that significant reinnervation errors can occur after lesions of the OS (Blanco-Hernández et al., 2012; Schwob, 2002; St John & Key, 2003). These errors presumably distort the olfactory information flow from the OE to the OB and higher olfactory centres (Costanzo & Miwa, 2006; Liu et al., 2021; Vedin et al., 2004; Yee & Costanzo, 1998). Depending on the type and degree of the peripheral lesions, particularly in mammals, the targeting errors can persist for extended periods (Calvo-Ochoa et al., 2021; Cheung et al., 2014; Schwob, 2002).

The fact that of the 15 odour-tuning response profiles found in the OB of non-transected *Xenopus* larvae, only 12 were present in larvae 3 weeks after ON transection supports our observation that the olfactory connections from the OE to the OB are still not completely and accurately reestablished at this point during regeneration (see Figure 3). Notably, most amine-responsive regions had not yet recovered. On the other hand, more bile acid-responsive regions were present if compared to control larvae. The frequency of occurrence of the remaining responsive regions did not notably change. This could indicate that amine-responsive ORNs regenerate slower than other ORN subclasses. In contrast, bile acid-responsive ORNs appear to regenerate faster and in excess. In the OS of mice, it has been shown that during the development of the OS, the timing of maturation of ORNs residing in different zones of the OE differs (Nishizumi & Sakano, 2015; Eerdunfu et al., 2017). In zebrafish, on the other hand, there is evidence that ORNs of different morphologies (ciliated vs. microvillous)

recover with varying speeds after damage to the OE (Calvo-Ochoa & Byrd-Jacobs, 2019; Ma et al., 2018). Our results indicate that ORN subclasses could have a different timing in regeneration also in *Xenopus* larvae.

Seven weeks after ON transection the segregation of cAMP-dependent and cAMP-independent ORN axons in the medial and lateral glomerular cluster, respectively, has nearly returned to control levels (see Figure 2). This shows that in the *Xenopus* OS, ORN axons of the medial and lateral odour processing streams rewire with considerable accuracy after ON transection. Also, all 15 odour-tuning response profiles found in non-transected control larvae were again present (see Figure 3). The frequency of amine-responsive regions that were diminished after 3 weeks of regeneration almost completely recovered. However, regions exclusively responsive to amines still were less frequent than in control animals. On the other hand, bile acid-responsive regions were still more frequent if compared to control larvae. Forskolin-sensitive areas were also slightly more frequent than in control animals.

The results discussed thus far show that in *X. laevis* larvae, axonal guidance mechanisms function during the regeneration after complete transection of the ON. Regenerating ORN axons of the two anatomically and functionally segregated odour processing streams find their way and reconnect to the original target areas in the OB. These observations imply that axonal guidance mechanisms are functional in both morphological ORN types, that is, microvillous and ciliated ORNs, endowed with different transduction cascades (Gliem et al., 2013). Several axonal guidance mechanisms have been shown to exist in the OS of other vertebrate species (for reviews, see Lodovichi, 2021; Mori & Sakano, 2011; Nishizumi & Sakano, 2015; Sakano, 2020). The axonal guidance mechanisms in *Xenopus* are unknown and need to be investigated in future studies.

Together, the functional calcium imaging experiments of the present study have shown that larval *Xenopus* exhibits accurate reinnervation of the OB by ORNs, accompanied by the recovery of odour-tuning response profiles in the OB, even after complete ON transection.

In rodents, the restoration of the OB network after damage or transection of the ON is less accurate. Although, in principle, reinnervation of the OB by ORN axons takes place, the resulting odour map in the OB is not accurately reformed (Christensen et al., 2001; Costanzo, 2000, 2005; Murai et al., 2016; Schwob, 2002). The recovery differences between amphibians and rodents may be due to the different time courses of ORN regeneration. In rodents, Murai and coworkers observed a complete loss of ORNs in the OE only 14 days after ON injury, and the reinnervation of the OB was still incomplete 42 days after injury (Murai et al., 2016). This caused a disruption of MTC dendritic connectivity that did not fully recover after 84 days (Murai et al., 2016). The resulting protracted loss of innervation to the OB likely leads to the loss of second-order neurons and interneurons, that is, the post-synaptic targets of ORN axons, that are lacking trophic support from the presynapse (Yu et al., 2004). In *Xenopus*, instead, ORNs already regenerate in the OE in 1 week (Hawkins et al., 2017), and thus, ORN axons probably reach the OB before a substantial loss of post-synaptic targets occurs.

### 4.3 | Behavioural responses to odourant stimuli are reestablished only after complete recovery of odour representations in the OB

To determine if and when, during the recovery process from ON transection, *X. laevis* larvae regain the ability to behaviourally respond to odors, we investigated odour-induced changes in behaviour in non-transected larvae and in larvae at different time points after ON transection. In our behavioural experiments, we employed amino acids as odourants. In aquatic species, amino acids are well-established odourants, and in various fish species, these stimuli have been shown to signal the presence of food and thus to attract animals (Hara, 2006; Olivares & Schmachtenberg, 2019; Valentinčič & Caprio, 1997). Amino acids are also suitable odourants in larval *Xenopus* (Gliem et al., 2013; Manzini et al., 2002; Manzini & Schild, 2010; Syed et al., 2017). When non-transected *Xenopus* larvae were exposed to amino acid odourants, their swimming velocity and the time they remained in the amino acid-enriched environment were affected (see Figure 4). We then determined if and at which point after ON transection the observed odour-induced behaviour returned during OS recovery. Although at 3 weeks after transection partial recovery seems to be present relative to ORN reinnervation and amino acid-induced activity in the OB (see Figures 2 and 3), we found that the recovery of olfactory guided behaviour only begins to occur within a 7–9-week range (see Figure 5). These experiments show that partial recovery of amino acid-induced responses in the OB is insufficient to recover odour-induced behaviour. Our behavioural results are in line with our earlier morphological results that showed that only starting from 7 weeks after ON transection, MTCs regained their glomerular tufts (Hawkins et al., 2017). These results also fit the functional calcium imaging results of the present study, which showed that a complete and precise recovery of odourant responses in the OB occurs only about

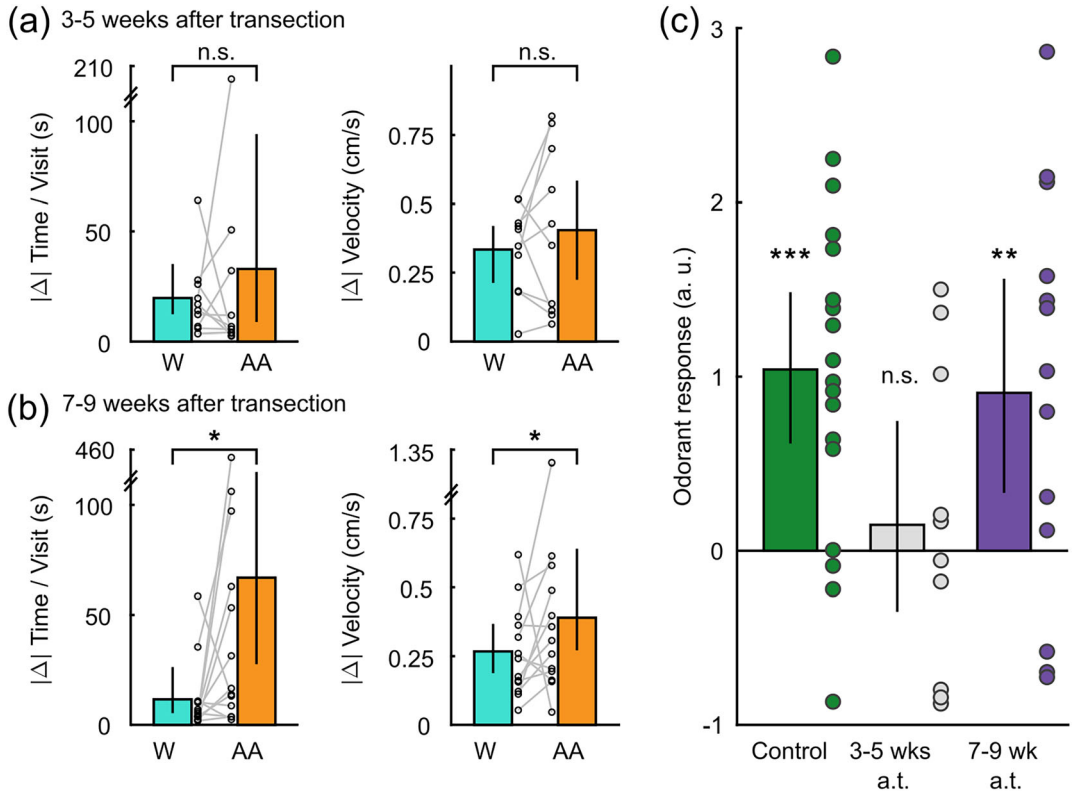


**FIGURE 5** Behavioral responses to odor stimuli in *Xenopus* larvae recover after ON transection. **(a).** Time per visit and velocity parameters in *Xenopus* larvae that had recovered 3–5 weeks after ON transection ($n = 10$ animals). Plots show the absolute value of the change from baseline computed as the normalised area under the curve (AUC) of the fitted log parabolic functions of time from the first entry in the W (blue) and AA (orange) areas. Error bars are 95% bootstrapped confidence intervals of the mean. Connected dots represent values for individual larvae. **(b).** Same as in a, for animals that had recovered 7–9 weeks after ON transection ($n = 13$ animals). **(c).** Combined time–velocity '*Odourant Response Index*' as a single parameter that shows the behavioural response to odor stimuli. Positive (>0) values signal a greater change in behaviour from baseline in the AA area compared to the W area. Bars are means, and error bars are 95% bootstrapped confidence intervals. Dots represent individual larvae. A significant behavioural response to odor stimuli can be seen in non-transected *Xenopus* larvae and larvae 7–9 weeks after ON transection. No significant response was found in larvae 3–5 weeks after ON transection. The control animals ($n = 18$) are the same as those tested in the experiments shown in Figure 4. AA, amino acids; n.s., not significant; W, water. $^{*}p < .05$; $^{**}p < .01$; $^{***}p < .001$.

7 weeks after ON transection. Together, our results show that only after a full functional reconnection of ORN axons with MTC dendrites can odourant information be adequately relayed to higher brain centres to initiate behavioural responses.

Using a similar lesion technique in which the ON was transected in both pre-metamorphic *X. laevis* and *Xenopus tropicalis* larvae, Terni et al. (2017) found that odour-guided behaviour no longer occurs in the days following the lesion but recovers already after 4 days. These authors found that the ON disappeared after the lesion but quickly reconnected to the OB after 3–4 days of recovery. Comparing anatomically defined glomeruli in non-transected larvae to glomeruli in larvae after ON transection, these authors found that new glomeruli could be identified after 8 days. After 15 days, the reformed glomeruli were similar to those found in non-transected animals. However, they suggest that the reformation of the glomeruli is not required to convey olfactory information to higher brain centres. Our results instead differ from those of Terni et al. (2017). We find that odour-guided behaviour only returns after the precise and functional reestablishment of the network of the OB and after reconnection of MTC to ORN axons in glomeruli (results of the present study and Hawkins et al., 2017).

The dissimilarities between our findings and those of Terni et al. (2017) could be due to several differences between the two studies. Specifically, Terni et al. (2017) used a different *Xenopus* species (*X. tropicalis*) and larvae of slightly different developmental stages (48–52) for their behavioural study. Further, Terni et al. employed slightly higher amino acid concentrations and a diverse amino acid mixture. Finally, they investigated behavioural responses occurring within 40 s of the initial exposure to

amino acids, whereas we investigated behavioural responses over a much longer time scale.

A fast return of olfactory-guided behaviour after ON transection has also been observed in goldfish (Hoyk et al., 1993; Zippel, 2000). In goldfish, it has been shown that after bilateral ON transection, regenerated ON fibres and terminals became again visible in the OB about 10 days to 2 weeks after transection. The same authors report that within the same timeframe after ON transection (10 days), odour-guided behaviour returns (von Rekowski & Zippel, 1993; Zippel, 2000). Similar results are found in zebrafish, where OB morphology is recovered in approximately 10 days following ORN ablation, and both glomerular innervation and olfactory-guided behaviour are restored within 3 weeks (Calvo-Ochoa et al., 2021). This suggests that OS regeneration may be faster in fishes than in *X. laevis* larvae.

In rodents, the situation is more complex. Several studies have shown that restoring olfactory-mediated behaviour following ON damage and transection is possible after approximately 40 days, and this coincides with the reinnervation of the OB (Harding & Wright, 1979; Yee & Costanzo, 1995, 1998). Additionally, ON transection in rodents leads to a distorted odour map in the OB (Costanzo, 2005; Murai et al., 2016; Schwob, 2002). Thus, the recovery of behavioural responses to odors in rodents may not be due to the reacquisition of accurate rewiring but rather resulting from a relearning and remapping of odourant stimuli during the process of bulbar reinnervation (Astic & Saucier, 2001).

## 5 | CONCLUSION

Across a series of calcium imaging and behavioural experiments, we have investigated the timing of the functional recovery of the OS after ON transection in larval *X. laevis*. We found that the OS regenerates with high accuracy, leading to the precise recovery of odourant-induced responses and odour-guided behaviour. It becomes increasingly evident that in earlier diverging vertebrates, including amphibians, the OS regenerates faster and more accurately than in mammalian species. Building on this evidence, in future studies, we will investigate which factors or mechanisms underlie the more favourable environment for regeneration in amphibians. These findings could be of potential clinical significance as they may lead to novel therapeutic approaches (Lledo & Valley, 2016; Shohayeb et al., 2018).

## AUTHOR CONTRIBUTIONS

**Sara Joy Hawkins:** Conceptualization; data curation; formal analysis; investigation; methodology; validation; writing—original draft; writing—review and editing. **Yvonne Gärtner:** Formal analysis; investigation; validation; writing—review and editing. **Thomas Offner:** Formal analysis; methodology; validation; writing—review and editing. **Lukas Weiss:** Formal analysis; methodology; validation; writing—review and editing. **Guido Maiello:** Formal analysis; validation; writing—review and editing. **Thomas Hassenklöver:** Conceptualization; supervision; validation; writing—original draft; writing—review and editing. **Ivan Manzini:** Conceptualization; funding acquisition; project administration; supervision; validation; writing—original draft; writing—review and editing.

## ACKNOWLEDGEMENTS

This work was supported by DFG (Grant 4113/4-1). Open Access funding enabled and organized by Projekt DEAL.

## CONFLICT OF INTEREST STATEMENT

The authors declare no competing interests.

## PEER REVIEW

The peer review history for this article is available at https://www.webofscience.com/api/gateway/wos/peer-review/10.1111/ejn.16375.

## DATA AVAILABILITY STATEMENT

Data and analysis scripts are available from the Zenodo database (doi: 10.5281/zenodo.10871200).

## ETHICAL STATEMENT

All animal procedures were performed following the guidelines of Laboratory animal research of the Institutional Care and Use Committee of the Justus Liebig University of Gießen (649_M; GI 15/7 Nr. G 89/2017; GI 15/3 Nr. G 15/2018; GI 15/7 kTV 7/2018; GI 15/7 Nr. G 2/2019).

## ORCID

*Sara J. Hawkins* https://orcid.org/0000-0002-7086-7262
*Thomas Offner* https://orcid.org/0000-0002-0228-2545
*Lukas Weiss* https://orcid.org/0000-0003-3078-8006
*Guido Maiello* https://orcid.org/0000-0001-6625-2583
*Thomas Hassenklöver* https://orcid.org/0000-0002-9895-1263
*Ivan Manzini* https://orcid.org/0000-0002-3575-9637

## REFERENCES

Ache, B. W., & Young, J. M. (2005). Olfaction: Diverse species, conserved principles. *Neuron*, *48*, 417–430. https://doi.org/10.1016/j.neuron.2005.10.022

Astic, L., & Saucier, D. (2001). Neuronal plasticity and regeneration in the olfactory system of mammals: Morphological and

functional recovery following olfactory bulb deafferentation. *Cellular and Molecular Life Sciences*, *58*, 538–545. https://doi.org/10.1007/PL00000879

Blanco-Hernández, E., Valle-Leija, P., Zomosa-Signoret, V., Drucker-Colín, R., & Vidaltamayo, R. (2012). Odor memory stability after reinnervation of the olfactory bulb. *PLoS ONE*, *7*, e46338. https://doi.org/10.1371/journal.pone.0046338

Brann, J. H., & Firestein, S. J. (2014). A lifetime of neurogenesis in the olfactory system. *Frontiers in Neuroscience*, *8*, 182. https://doi.org/10.3389/fnins.2014.00182

Breer, H. (2003). Olfactory receptors: Molecular basis for recognition and discrimination of odors. *Analytical and Bioanalytical Chemistry*, *377*, 427–433. https://doi.org/10.1007/s00216-003-2113-9

Buck, L., & Axel, R. (1991). A novel multigene family may encode odorant receptors: A molecular basis for odor recognition. *Cell*, *65*, 175–187. https://doi.org/10.1016/0092-8674(91)90418-X

Buck, L. B. (1996). Information coding in the vertebrate olfactory system. *Annual Review of Neuroscience*, *19*, 517–544. https://doi.org/10.1146/annurev.ne.19.030196.002505

Burton, S. D., Brown, A., Eiting, T. P., Youngstrom, I. A., Rust, T. C., Schmuker, M., & Wachowiak, M. (2022). Mapping odorant sensitivities reveals a sparse but structured representation of olfactory chemical space by sensory input to the mouse olfactory bulb. *eLife*, *11*, e80470. https://doi.org/10.7554/eLife.80470

Calvo-Ochoa, E., & Byrd-Jacobs, C. A. (2019). The olfactory system of zebrafish as a model for the study of neurotoxicity and injury: Implications for neuroplasticity and disease. *International Journal of Molecular Sciences*, *20*, 1639. https://doi.org/10.3390/ijms20071639

Calvo-Ochoa, E., Byrd-Jacobs, C. A., & Fuss, S. H. (2021). Diving into the streams and waves of constitutive and regenerative olfactory neurogenesis: Insights from zebrafish. *Cell and Tissue Research*, *383*, 227–253. https://doi.org/10.1007/s00441-020-03334-2

Caprio, J., & Byrd, R. P. (1984). Electrophysiological evidence for acidic, basic, and neutral amino acid olfactory receptor sites in the catfish. *Journal of General Physiology*, *84*, 403–422. https://doi.org/10.1085/jgp.84.3.403

Carr, W. E. S., & Derby, C. D. (1986). Chemically stimulated feeding behavior in marine animals: Importance of chemical mixtures and involvement of mixture interactions. *Journal of Chemical Ecology*, *12*, 989–1011. https://doi.org/10.1007/BF01638992

Carr, W. E. S., Gleeson, R. A., & Trapido-Rosenthal, H. G. (1990). The role of perireceptor events in chemosensory processes. *Trends in Neurosciences*, *13*, 212–215. https://doi.org/10.1016/0166-2236(90)90162-4

Cheung, M. C., Jang, W., Schwob, J. E., & Wachowiak, M. (2014). Functional recovery of odor representations in regenerated sensory inputs to the olfactory bulb. *Frontiers in Neural Circuits*, *7*, 207. https://doi.org/10.3389/fncir.2013.00207

Christensen, M. D., Holbrook, E. H., Costanzo, R. M., & Schwob, J. E. (2001). Rhinotopy is disrupted during the reinnervation of the olfactory bulb that follows transection of the olfactory nerve. *Chemical Senses*, *26*, 359–369. https://doi.org/10.1093/chemse/26.4.359

Costanzo, R. M. (2000). Rewiring the olfactory bulb: Changes in odor maps following recovery from nerve transection. *Chemical Senses*, *25*, 199–205. https://doi.org/10.1093/chemse/25.2.199

Costanzo, R. M. (2005). Regeneration and rewiring the olfactory bulb. *Chemical Senses*, *30*, i133–i134. https://doi.org/10.1093/chemse/bjh150

Costanzo, R. M., & Miwa, T. (2006). Posttraumatic olfactory loss. *Advances in Oto-Rhino-Laryngology*, *63*, 99–107. https://doi.org/10.1159/000093753

Cowan, C. M., & Roskams, A. J. (2002). Apoptosis in the mature and developing olfactory neuroepithelium. *Microscopy Research and Technique*, *58*, 204–215. https://doi.org/10.1002/jemt.10150

Czesnik, D., Kuduz, J., Schild, D., & Manzini, I. (2006). ATP activates both receptor and sustentacular supporting cells in the olfactory epithelium of Xenopus laevis tadpoles. *European Journal of Neuroscience*, *23*, 119–128. https://doi.org/10.1111/j.1460-9568.2005.04533.x

De Franceschi, G., Vivattanasarn, T., Saleem, A. B., & Solomon, S. G. (2016). Vision guides selection of freeze or flight defense strategies in mice. *Current Biology*, *26*, 2150–2154. https://doi.org/10.1016/j.cub.2016.06.006

Dikecligil, G. N., & Gottfried, J. A. (2024). What does the human olfactory system do, and how does it do it? *Annual Review of Psychology*, *75, null*, 155–181. https://doi.org/10.1146/annurev-psych-042023-101155

Dittrich, K., Kuttler, J., Hassenklöver, T., & Manzini, I. (2016). Metamorphic remodeling of the olfactory organ of the African clawed frog, Xenopus laevis. *Journal of Comparative Neurology*, *524*, 986–998. https://doi.org/10.1002/cne.23887

Eerdunfu, Ihara, N., Ligao, B., Ikegaya, Y., & Takeuchi, H. (2017). Differential timing of neurogenesis underlies dorsal–ventral topographic projection of olfactory sensory neurons. *Neural Development*, *12*, 2. https://doi.org/10.1186/s13064-017-0079-0

Eilers, P. H., & Boelens, H. F. (2005). Baseline correction with asymmetric least squares smoothing. *Leiden University Medical Centre Report*, *1*, 5.

Eisthen, H. L. (2002). Why are olfactory systems of different animals so similar? *Brain, Behavior and Evolution*, *59*, 273–293. https://doi.org/10.1159/000063564

Frasnelli, J., Laguë-Beauvais, M., LeBlanc, J., Alturki, A. Y., Champoux, M. C., Couturier, C., Anderson, K., Lamoureux, J., Marcoux, J., Tinawi, S., Dagher, J., Maleki, M., Feyz, M., & de Guise, E. (2016). Olfactory function in acute traumatic brain injury. *Clinical Neurology and Neurosurgery*, *140*, 68–72. https://doi.org/10.1016/j.clineuro.2015.11.013

Friedrich, J., Zhou, P., & Paninski, L. (2017). Fast online deconvolution of calcium imaging data. *PLoS Computational Biology*, *13*, e1005423. https://doi.org/10.1371/journal.pcbi.1005423

Frontera, J. L., Raices, M., Cervino, A. S., Pozzi, A. G., & Paz, D. A. (2016). Neural regeneration dynamics of *Xenopus laevis* olfactory epithelium after zinc sulfate-induced damage. *Journal of Chemical Neuroanatomy*, *77*, 1–9. https://doi.org/10.1016/j.jchemneu.2016.02.003

Gaillard, I., Rouquier, S., & Giorgi, D. (2004). Olfactory receptors. *Cellular and Molecular Life Sciences (CMLS)*, *61*, 456–469. https://doi.org/10.1007/s00018-003-3273-7

Giovannucci, A., Friedrich, J., Gunn, P., Kalfon, J., Brown, B. L., Koay, S. A., Taxidis, J., Najafi, F., Gauthier, J. L., Zhou, P., Khakh, B. S., Tank, D. W., Chklovskii, D. B., &

Pnevmatikakis, E. A. (2019). CaImAn an open source tool for scalable calcium imaging data analysis. *eLife*, *8*, e38173. https://doi.org/10.7554/eLife.38173

Gliem, S., Schild, D., & Manzini, I. (2009). Highly specific responses to amine odorants of individual olfactory receptor neurons in situ. *European Journal of Neuroscience*, *29*, 2315–2326. https://doi.org/10.1111/j.1460-9568.2009.06778.x

Gliem, S., Syed, A. S., Sansone, A., Kludt, E., Tantalaki, E., Hassenklöver, T., Korsching, S. I., & Manzini, I. (2013). Bimodal processing of olfactory information in an amphibian nose: Odor responses segregate into a medial and a lateral stream. *Cellular and Molecular Life Sciences*, *70*, 1965–1984. https://doi.org/10.1007/s00018-012-1226-8

Godoy, R., Hua, K., Kalyn, M., Cusson, V.-M., Anisman, H., & Ekker, M. (2020). Dopaminergic neurons regenerate following chemogenetic ablation in the olfactory bulb of adult zebrafish (*Danio rerio*). *Scientific Reports*, *10*, 12825. https://doi.org/10.1038/s41598-020-69734-0

Grabe, V., & Sachse, S. (2018). Fundamental principles of the olfactory code. *Biosystems, Code Biology*, *164*, 94–101. https://doi.org/10.1016/j.biosystems.2017.10.010

Graziadei, P. P. C. (1973). Cell dynamics in the olfactory mucosa. *Tissue and Cell*, *5*, 113–131. https://doi.org/10.1016/S0040-8166(73)80010-2

Graziadei, P. P. C., & DeHan, R. S. (1973). Neuronal regeneration in frog olfactory system. *Journal of Cell Biology*, *59*, 525–530. https://doi.org/10.1083/jcb.59.2.525

Graziadei, P. P. C., & Metcalf, J. F. (1971). Autoradiographic and ultrastructural observations on the frog's olfactory mucosa. *Zeitschrift für Zellforschung und Mikroskopische Anatomie*, *116*, 305–318. https://doi.org/10.1007/BF00330630

Graziadei, P. P. C., & Monti Graziadei, G. A. (1980). Neurogenesis and neuron regeneration in the olfactory system of mammals. III. Deafferentation and reinnervation of the olfactory bulb following section of the*fila olfactoria* in rat. *Journal of Neurocytology*, *9*, 145–162. https://doi.org/10.1007/BF01205155

Hahn, C.-G., Han, L.-Y., Rawson, N. E., Mirza, N., Borgmann-Winter, K., Lenox, R. H., & Arnold, S. E. (2005). In vivo and in vitro neurogenesis in human olfactory epithelium. *The Journal of Comparative Neurology*, *483*, 154–163. https://doi.org/10.1002/cne.20424

Hänzi, S., & Straka, H. (2018). Wall following in *Xenopus laevis* is barrier-driven. *Journal of Comparative Physiology A*, *204*, 183–195. https://doi.org/10.1007/s00359-017-1227-z

Hara, T. J. (2006). Feeding behaviour in some teleosts is triggered by single amino acids primarily through olfaction. *Journal of Fish Biology*, *68*, 810–825. https://doi.org/10.1111/j.0022-1112.2006.00967.x

Harding, J. W., & Wright, J. W. (1979). Reversible effects of olfactory nerve section on behavior and biochemistry in mice. *Brain Research Bulletin*, *4*, 17–22. https://doi.org/10.1016/0361-9230(79)90053-4

Hawkins, S. J., Weiss, L., Offner, T., Dittrich, K., Hassenklöver, T., & Manzini, I. (2017). Functional reintegration of sensory neurons and transitional dendritic reduction of mitral/tufted cells during injury-induced recovery of the larval *Xenopus* olfactory circuit. *Frontiers in Cellular Neuroscience*, *11*, 380. https://doi.org/10.3389/fncel.2017.00380

Howell, J., Costanzo, R. M., & Reiter, E. R. (2018). Head trauma and olfactory function. *World Journal of Otorhinolaryngology—Head and Neck Surgery*, *4*, 39–45. https://doi.org/10.1016/j.wjorl.2018.02.001

Hoyk, Z., Lago-Schaaf, T., Zippel, H. P., Füzesi, G., & Halász, N. (1993). Fast regeneration of the olfactory nerve in goldfish: Fine structure and behaviour. *Journal Fur Hirnforschung*, *34*, 461–465.

Jafari, A., & Holbrook, E. H. (2022). Therapies for olfactory dysfunction—An update. *Current Allergy and Asthma Reports*, *22*, 21–28. https://doi.org/10.1007/s11882-022-01028-z

Jennings, R. A., Hambright Keiger, C. J., & Walker, J. C. (1995). Time course of reinnervation of the olfactory bulb after transection of the primary olfactory nerve in the pigeon. *Brain Research*, *683*, 159–163. https://doi.org/10.1016/0006-8993(95)00361-S

Jiang, R.-S., & Lu, Y.-Y. (2019). Functional olfactory nerve regeneration demonstrated by Thallium-201 olfacto-scintigraphy in patients with traumatic anosmia: A case report. *Case Reports in Otolaryngology*, *2019*, e1069741. https://doi.org/10.1155/2019/1069741

Johnson, B. A., & Leon, M. (2007). Chemotopic odorant coding in a mammalian olfactory system. *Journal of Comparative Neurology*, *503*, 1–34. https://doi.org/10.1002/cne.21396

Kang, J., & Caprio, J. (1995). In vivo responses of single olfactory receptor neurons in the channel catfish, Ictalurus punctatus. *Journal of Neurophysiology*, *73*, 172–177. https://doi.org/10.1152/jn.1995.73.1.172

Kobayashi, M., & Costanzo, R. M. (2009). Olfactory nerve recovery following mild and severe injury and the efficacy of dexamethasone treatment. *Chemical Senses*, *34*, 573–580. https://doi.org/10.1093/chemse/bjp038

Koster, N. L., & Costanzo, R. M. (1996). Electrophysiological characterization of the olfactory bulb during recovery from sensory deafferentation. *Brain Research*, *724*, 117–120. https://doi.org/10.1016/0006-8993(96)00281-8

Leung, C. T., Coulombe, P. A., & Reed, R. R. (2007). Contribution of olfactory neural stem cells to tissue maintenance and regeneration. *Nature Neuroscience*, *10*, 720–726. https://doi.org/10.1038/nn1882

Lim, D. A., & Alvarez-Buylla, A. (2016). The adult ventricular–subventricular zone (V-SVZ) and olfactory bulb (OB) neurogenesis. *Cold Spring Harbor Perspectives in Biology*, *8*, a018820. https://doi.org/10.1101/cshperspect.a018820

Liu, D. T., Sabha, M., Damm, M., Philpott, C., Oleszkiewicz, A., Hähner, A., & Hummel, T. (2021). Parosmia is associated with relevant olfactory recovery after olfactory training. *The Laryngoscope*, *131*, 618–623. https://doi.org/10.1002/lary.29277

Lledo, P.-M., & Valley, M. (2016). Adult olfactory bulb neurogenesis. *Cold Spring Harbor Perspectives in Biology*, *8*, a018945. https://doi.org/10.1101/cshperspect.a018945

Lodovichi, C. (2021). Topographic organization in the olfactory bulb. *Cell and Tissue Research*, *383*, 457–472. https://doi.org/10.1007/s00441-020-03348-w

Ma, E. Y., Heffern, K., Cheresh, J., & Gallagher, E. P. (2018). Differential copper-induced death and regeneration of olfactory sensory neuron populations and neurobehavioral function in larval zebrafish. *Neurotoxicology*, *69*, 141–151. https://doi.org/10.1016/j.neuro.2018.10.002

Manzini, I. (2015). From neurogenesis to neuronal regeneration: The amphibian olfactory system as a model to visualize

neuronal development: In vivo. *Neural Regeneration Research*, *10*, 872–874. https://doi.org/10.4103/1673-5374.158334

Manzini, I., Brase, C., Chen, T.-W., & Schild, D. (2007). Response profiles to amino acid odorants of olfactory glomeruli in larval *Xenopus laevis*. *The Journal of Physiology*, *581*, 567–579. https://doi.org/10.1113/jphysiol.2007.130518

Manzini, I., Heermann, S., Czesnik, D., Brase, C., Schild, D., & Rössler, W. (2007). Presynaptic protein distribution and odour mapping in glomeruli of the olfactory bulb of Xenopus laevis tadpoles: Odour mapping in glomerular clusters. *European Journal of Neuroscience*, *26*, 925–934. https://doi.org/10.1111/j.1460-9568.2007.05731.x

Manzini, I., Rössler, W., & Schild, D. (2002). cAMP-independent responses of olfactory neurons in *Xenopus laevis* tadpoles and their projection onto olfactory bulb neurons. *The Journal of Physiology*, *545*, 475–484. https://doi.org/10.1113/jphysiol.2002.031914

Manzini, I., & Schild, D. (2003). cAMP-independent olfactory transduction of amino acids in *Xenopus laevis* tadpoles. *The Journal of Physiology*, *551*, 115–123. https://doi.org/10.1113/jphysiol.2003.043059

Manzini, I., & Schild, D. (2004). Classes and narrowing selectivity of olfactory receptor neurons of *Xenopus laevis* tadpoles. *Journal of General Physiology*, *123*, 99–107. https://doi.org/10.1085/jgp.200308970

Manzini, I. & Schild, D. (2010) Olfactory coding in larvae of the African clawed frog *Xenopus laevis*. In Menini, A. (ed), *The neurobiology of olfaction*, Frontiers in Neuroscience. CRC Press/Taylor & Francis, https://doi.org/10.1201/9781420071993-c4

Manzini, I., Schild, D., & Di Natale, C. (2022). Principles of odor coding in vertebrates and artificial chemosensory systems. *Physiological Reviews*, *102*, 61–154. https://doi.org/10.1152/physrev.00036.2020

McMillan Carr, V., Ring, G., Youngentob, S. L., Schwob, J. E., & Farbman, A. I. (2004). Altered epithelial density and expansion of bulbar projections of a discrete HSP70 immunoreactive subpopulation of rat olfactory receptor neurons in reconstituting olfactory epithelium following exposure to methyl bromide. *The Journal of Comparative Neurology*, *469*, 475–493. https://doi.org/10.1002/cne.11020

Mombaerts, P., Wang, F., Dulac, C., Chao, S. K., Nemes, A., Mendelsohn, M., Edmondson, J., & Axel, R. (1996). Visualizing an olfactory sensory map. *Cell*, *87*, 675–686. https://doi.org/10.1016/S0092-8674(00)81387-2

Mori, K., & Sakano, H. (2011). How is the olfactory map formed and interpreted in the mammalian brain? *Annual Review of Neuroscience*, *34*, 467–499. https://doi.org/10.1146/annurev-neuro-112210-112917

Mulvaney, B. D., & Heist, H. E. (1971). Regeneration of rabbit olfactory epithelium. *American Journal of Anatomy*, *131*, 241–251. https://doi.org/10.1002/aja.1001310208

Murai, A., Iwata, R., Fujimoto, S., Aihara, S., Tsuboi, A., Muroyama, Y., Saito, T., Nishizaki, K., & Imai, T. (2016). Distorted coarse axon targeting and reduced dendrite connectivity underlie dysosmia after olfactory axon injury. *Eneuro*, *3*, ENEURO.0242-16.2016. https://doi.org/10.1523/ENEURO.0242-16.2016

Murray, R. C., & Calof, A. L. (1999). Neuronal regeneration: Lessons from the olfactory system. *Seminars in Cell & Developmental Biology*, *10*, 421–431. https://doi.org/10.1006/scdb.1999.0329

Nakamuta, S., Nakamuta, N., & Taniguchi, K. (2011). Distinct axonal projections from two types of olfactory receptor neurons in the middle chamber epithelium of *Xenopus laevis*. *Cell and Tissue Research*, *346*, 27–33. https://doi.org/10.1007/s00441-011-1238-y

Nezlin, L. P., & Schild, D. (2000). Structure of the olfactory bulb in tadpoles of *Xenopus laevis*. *Cell and Tissue Research*, *302*, 21–29. https://doi.org/10.1007/s004410000208

Nieuwkoop, P. D., & Faber, J. (1994). *Normal table of* Xenopus Laevis *(Daudin): A systematical and chronological survey of the development from the fertilized egg till the end of metamorphosis*. Garland Pub.

Nishizumi, H., & Sakano, H. (2015). Developmental regulation of neural map formation in the mouse olfactory system. *Developmental Neurobiology*, *75*, 594–607. https://doi.org/10.1002/dneu.22268

Offner, T., Daume, D., Weiss, L., Hassenklöver, T., & Manzini, I. (2020). Whole-brain calcium imaging in larval *Xenopus*. *Cold Spring Harbor Protocols*. https://doi.org/10.1101/pdb.prot106815

Offner, T., Weiss, L., Daume, D., Berk, A., Inderthal, T. J., Manzini, I., & Hassenklöver, T. (2023). Functional odor map heterogeneity is based on multifaceted glomerular connectivity in larval *Xenopus* olfactory bulb. *iScience*, *26*(9), 107518. https://doi.org/10.1016/j.isci.2023.107518

Oley, N., DeHan, R. S., Tucker, D., Smith, J. C., & Graziadei, P. P. C. (1975). Recovery of structure and function following transection of the primary olfactory nerves in pigeons. *Journal of Comparative and Physiological Psychology*, *88*, 477–495. https://doi.org/10.1037/h0076401

Olivares, J., & Schmachtenberg, O. (2019). An update on anatomy and function of the teleost olfactory system. *PeerJ*, *7*, e7808. https://doi.org/10.7717/peerj.7808

Pastore, M., & Calcagnì, A. (2019). Measuring distribution similarities between samples: A distribution-free overlapping index. *Frontiers in Psychology*, *10*, 1089. https://doi.org/10.3389/fpsyg.2019.01089

Pnevmatikakis, E. A., & Giovannucci, A. (2017). NoRMCorre: An online algorithm for piecewise rigid motion correction of calcium imaging data. *Journal of Neuroscience Methods*, *291*, 83–94. https://doi.org/10.1016/j.jneumeth.2017.07.031

Poncelet, G., & Shimeld, S. M. (2020). The evolutionary origins of the vertebrate olfactory system. *Open Biology*, *10*, 200330. https://doi.org/10.1098/rsob.200330

Reiter, E. R., DiNardo, L. J., & Costanzo, R. M. (2004). Effects of head injury on olfaction and taste. *Otolaryngologic Clinics of North America, Olfaction and Taste*, *37*, 1167–1184. https://doi.org/10.1016/j.otc.2004.06.005

Ressler, K. J., Sullivan, S. L., & Buck, L. B. (1994). Information coding in the olfactory system: Evidence for a stereotyped and highly organized epitope map in the olfactory bulb. *Cell*, *79*, 1245–1255. https://doi.org/10.1016/0092-8674(94)90015-9

Rolen, S. H., Sorensen, P. W., Mattson, D., & Caprio, J. (2003). Polyamines as olfactory stimuli in the goldfish *Carassius* auratus. *Journal of Experimental Biology*, *206*, 1683–1696. https://doi.org/10.1242/jeb.00338

Sakano, H. (2020). Developmental regulation of olfactory circuit formation in mice. *Development, Growth & Differentiation*, *62*, 199–213. https://doi.org/10.1111/dgd.12657

Sansone, A., Hassenklöver, T., Syed, A. S., Korsching, S. I., & Manzini, I. (2014). Phospholipase C and diacylglycerol mediate olfactory responses to amino acids in the main olfactory epithelium of an amphibian. *PLoS ONE*, *9*, e87721. https://doi.org/10.1371/journal.pone.0087721

Sato, K., & Suzuki, N. (2001). Whole-cell response characteristics of ciliated and microvillous olfactory receptor neurons to amino acids, pheromone candidates and urine in rainbow trout. *Chemical Senses*, *26*, 1145–1156. https://doi.org/10.1093/chemse/26.9.1145

Sato, Y., Miyasaka, N., & Yoshihara, Y. (2005). Mutually exclusive glomerular innervation by two distinct types of olfactory sensory neurons revealed in transgenic zebrafish. *Journal of Neuroscience*, *25*, 4889–4897. https://doi.org/10.1523/JNEUROSCI.0679-05.2005

Schild, D., & Manzini, I. (2004). Cascades of response vectors of olfactory receptor neurons in *Xenopus laevis* tadpoles. *European Journal of Neuroscience*, *20*, 2111–2123. https://doi.org/10.1111/j.1460-9568.2004.03672.x

Schwob, J. E. (2002). Neural regeneration and the peripheral olfactory system. *The Anatomical Record*, *269*, 33–49. https://doi.org/10.1002/ar.10047

Schwob, J. E., Jang, W., Holbrook, E. H., Lin, B., Herrick, D. B., Peterson, J. N., & Hewitt Coleman, J. (2017). Stem and progenitor cells of the mammalian olfactory epithelium: Taking poietic license: Stem and progenitor cells of the mammalian OE. *Journal of Comparative Neurology*, *525*, 1034–1054. https://doi.org/10.1002/cne.24105

Schwob, J. E., Youngentob, S. L., Ring, G., Iwema, C. L., & Mezza, R. C. (1999). Reinnervation of the rat olfactory bulb after methyl bromide-induced lesion: Timing and extent of reinnervation. *The Journal of Comparative Neurology*, *412*, 439–457. https://doi.org/10.1002/(SICI)1096-9861(19990927)412:3<439::AID-CNE5>3.0.CO;2-H

Scott, D. W. (1992). *Multivariate density estimation: Theory, practice, and visualization* (1st ed. edn, Wiley Series in Probability and Statistics). Wiley. https://doi.org/10.1002/9780470316849

Shohayeb, B., Diab, M., Ahmed, M., & Ng, D. C. H. (2018). Factors that influence adult neurogenesis as potential therapy. *Translational Neurodegeneration*, *7*, 4. https://doi.org/10.1186/s40035-018-0109-9

Simmons, P. A., & Getchell, T. V. (1981a). Neurogenesis in olfactory epithelium: Loss and recovery of transepithelial voltage transients following olfactory nerve section. *Journal of Neurophysiology*, *45*, 516–528. https://doi.org/10.1152/jn.1981.45.3.516

Simmons, P. A., & Getchell, T. V. (1981b). Physiological activity of newly differentiated olfactory receptor neurons correlated with morphological recovery from olfactory nerve section in the salamander. *Journal of Neurophysiology*, *45*, 529–549. https://doi.org/10.1152/jn.1981.45.3.529

Simmons, P. A., Rafols, J. A., & Getchell, T. V. (1981). Ultrastructural changes in olfactory receptor neurons following olfactory nerve section. *Journal of Comparative Neurology*, *197*, 237–257. https://doi.org/10.1002/cne.901970206

Sokpor, G., Abbas, E., Rosenbusch, J., Staiger, J. F., & Tuoc, T. (2018). Transcriptional and epigenetic control of mammalian olfactory epithelium development. *Molecular Neurobiology*, *55*, 8306–8327. https://doi.org/10.1007/s12035-018-0987-y

Spehr, M., & Munger, S. D. (2009). Olfactory receptors: G protein-coupled receptors and beyond. *Journal of Neurochemistry*, *109*, 1570–1583. https://doi.org/10.1111/j.1471-4159.2009.06085.x

St John, J. A., & Key, B. (2003). Axon mis-targeting in the olfactory bulb during regeneration of olfactory Neuroepithelium. *Chemical Senses*, *28*, 773–779. https://doi.org/10.1093/chemse/bjg068

Syed, A. S., Sansone, A., Hassenklöver, T., Manzini, I., & Korsching, S. I. (2017). Coordinated shift of olfactory amino acid responses and V2R expression to an amphibian water nose during metamorphosis. *Cellular and Molecular Life Sciences*, *74*, 1711–1719. https://doi.org/10.1007/s00018-016-2437-1

Terni, B., Pacciolla, P., Masanas, H., Gorostiza, P., & Llobet, A. (2017). Tight temporal coupling between synaptic rewiring of olfactory glomeruli and the emergence of odor-guided behavior in *Xenopus* tadpoles. *Journal of Comparative Neurology*, *525*, 3769–3783. https://doi.org/10.1002/cne.24303

Tufo, C., Poopalasundaram, S., Dorrego-Rivas, A., Ford, M. C., Graham, A., & Grubb, M. S. (2022). Development of the mammalian main olfactory bulb. *Development*, *149*, dev200210. https://doi.org/10.1242/dev.200210

Valentinčič, T., & Caprio, J. (1997). Visual and chemical release of feeding behavior in adult rainbow trout. *Chemical Senses*, *22*, 375–382. https://doi.org/10.1093/chemse/22.4.375

Vedin, V., Slotnick, B., & Berghard, A. (2004). Zonal ablation of the olfactory sensory neuroepithelium of the mouse: Effects on odorant detection. *European Journal of Neuroscience*, *20*, 1858–1864. https://doi.org/10.1111/j.1460-9568.2004.03634.x

Virtanen, P., Gommers, R., Oliphant, T. E., Haberland, M., Reddy, T., Cournapeau, D., Burovski, E., Peterson, P., Weckesser, W., Bright, J., van der Walt, S. J., Brett, M., Wilson, J., Millman, K. J., Mayorov, N., Nelson, A. R. J., Jones, E., Kern, R., Larson, E., … Vázquez-Baeza, Y. (2020). SciPy 1.0: Fundamental algorithms for scientific computing in Python. *Nature Methods*, *17*, 261–272. https://doi.org/10.1038/s41592-019-0686-2

von Rekowski, C., & Zippel, H. P. (1993). In goldfish the qualitative discriminative ability for odors rapidly returns after bilateral nerve axotomy and lateral olfactory tract transection. *Brain Research*, *618*, 338–340. https://doi.org/10.1016/0006-8993(93)91287-3

Weiss, L., Manzini, I., & Hassenklöver, T. (2021). Olfaction across the water–air interface in anuran amphibians. *Cell and Tissue Research*, *383*, 301–325. https://doi.org/10.1007/s00441-020-03377-5

Weiss, L., Offner, T., Hassenklöver, T., & Manzini, I. (2018). Dye electroporation and imaging of calcium signaling in *Xenopus* nervous system. In K. Vleminckx (Ed.), *Xenopus* (pp. 217–231). Springer. https://doi.org/10.1007/978-1-4939-8784-9_15

Weiss, L., Segoviano Arias, P., Offner, T., Hawkins, S. J., Hassenklöver, T., & Manzini, I. (2021). Distinct interhemispheric connectivity at the level of the olfactory bulb emerges during *Xenopus laevis* metamorphosis. *Cell and Tissue Research*, *386*, 491–511. https://doi.org/10.1007/s00441-021-03527-3

Whitcroft, K. L., Altundag, A., Balungwe, P., Boscolo-Rizzo, P., Douglas, R., Enecilla, M. L. B., Fjaeldstad, A. W., Fornazieri, M. A., Frasnelli, J., Gane, S., Gudziol, H., Gupta, N., Haehner, A., Hernandez, A. K., Holbrook, E. H., Hopkins, C., Hsieh, J. W., Huart, C., Husain, S., … Hummel, T. (2023). Position paper on olfactory dysfunction: 2023. *Rhinology*, *61*, 1–131. https://doi.org/10.4193/Rhin22.483

Yee, K. K., & Costanzo, R. M. (1995). Restoration of olfactory mediated behavior after olfactory bulb deafferentation. *Physiology & Behavior*, *58*, 959–968. https://doi.org/10.1016/0031-9384(95)00159-G

Yee, K. K., & Costanzo, R. M. (1998). Changes in odor quality discrimination following recovery from olfactory nerve transection. *Chemical Senses*, *23*, 513–519. https://doi.org/10.1093/chemse/23.5.513

Yu, C. R., Power, J., Barnea, G., O'Donnell, S., Brown, H. E. V., Osborne, J., Axel, R., & Gogos, J. A. (2004). Spontaneous neural activity is required for the establishment and maintenance of the olfactory sensory map. *Neuron*, *42*, 553–566. https://doi.org/10.1016/S0896-6273(04)00224-7

Zippel, H. P. (2000). In goldfish the discriminative ability for odours persists after reduction of the olfactory epithelium, and rapidly returns after olfactory nerve axotomy and crossing bulbs. *Philosophical Transactions of the Royal Society of London. Series B: Biological Sciences*, *355*, 1219–1223.

**How to cite this article:** Hawkins, S. J., Gärtner, Y., Offner, T., Weiss, L., Maiello, G., Hassenklöver, T., & Manzini, I. (2024). The olfactory network of larval *Xenopus laevis* regenerates accurately after olfactory nerve transection. *European Journal of Neuroscience*, *60*(1), 3719–3741. https://doi.org/10.1111/ejn.16375